Doctoral Dissertation

Studies on the Effects of Acid Anhydrides-Modified Cellulose Nanofibers as Filler in Transparent Plastic Composites

酸無水物変性セルロースナノファイバーをフィラーとして用いた透明プラスチック複合材料に関する研究

NAHARULLAH BIN JAMALUDDIN

June 2021

Graduate School of Engineering

Osaka University

Contents

Chapter 3

Acylation of Cellulose Nanofiber as Filler for Poly(methyl methacrylate) Composite Films Reinforcement

General Introduction

Plastic polymers are low-cost, lightweight, sturdy, long-lasting, corrosion-resistant materials with excellent thermal and electrical insulation.[1] Polymers' versatility and variety of properties are used to create wide applications such as medical and technical advancements, energy conservation, and many other social benefits.[1–3] Plastics are used in almost every aspect of everyday life, including transportation, telecommunications, garments, boots, and as packing materials to allow the transportation of a wide variety of food, drink, and other products. Plastics have a lot of potentials for the new technologies that can help people in the future, such as green energy generation, medical applications, and energy reduction for transportation.[1] The use of raw plastic or polymers is uncommon, and most polymer resins are blended with various additives to enhance their properties. Polymer products that depend on fossil resources have been an essential part of industry and people's everyday lives. This is because of their outstanding resilience, high power, and ease of manufacturing. However, the resource and environmental issues portrayed by their non-renewability and non-biodegradability have caused the public to recognize the significance and requirement of developing natural polymer-based products.[4,5] Natural fiber biopolymers have recently gained popularity as an environmentally friendly alternative to conventional polymers.[6]

Cellulose is the most common natural polymer on the earth, as well as the cheapest and most widely available. It is biodegradable, biocompatible, and has a wide range of chemical modification capabilities.[7,8] Based on the desired use, cellulose can be processed into a variety of sizes. Micro- and nano-sized cellulose are the most common cellulose sizes used in laboratories and industrial applications. There are three types of nanocellulose, which are, cellulose nanofiber (CNF), cellulose nanocrystal (CNC), and bacterial cellulose (BC).[9,10] The fiber size distributions

vary between CNF and CNC, which are broad in CNF and significantly shorter or narrow in CNC.[11] BC, which harvested from tunicates has a narrow size distribution and high crystallinity. According to Chirayil et al., CNF and CNC are well-known for their biodegradability, superior properties, distinctive architectures, low density, excellent mechanical performance, high surface area and aspect ratio, biocompatibility, and natural abundance.[12] The benefit of isolating or extracting cellulose is that nanocellulose can be generated from microcellulose, resulting in various cellulose sizes in a compatible process (**Figure 2**).[13] Sizes of nanocellulose can vary between 5 and 100 nm in diameter.[14] The difference between CNF and microfibrillated cellulose (MFC) is that CNF is typically generated by high-pressure homogenization, while MFC is typically produced through chemical treatment.[15] Wood, potato, hemp, and flax are among the sources of CNF or MFC and their average diameter is between 20–50 nm.[16,17] Meanwhile, the average diameter and length for CNC are 5–70 nm and 100 nm, respectively.[4] CNC is extracted from wood, cotton, hemp, and flax, with additional sources from wheat straw, bark, algae and bacteria, and animals (tunicates).[18] Other than CNC, BC also is extracted from non-plant, which are tunicates as mentioned earlier. The use of microorganisms in the biopolymer industry is important because they naturally grow quickly, hence, allowing higher yields and year-round productibility.[19]

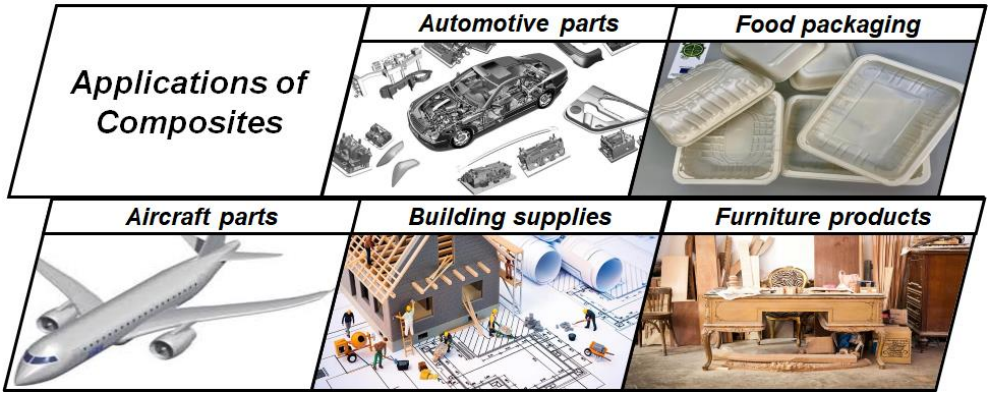

Figure 1. Variety of composites' uses in several industries.

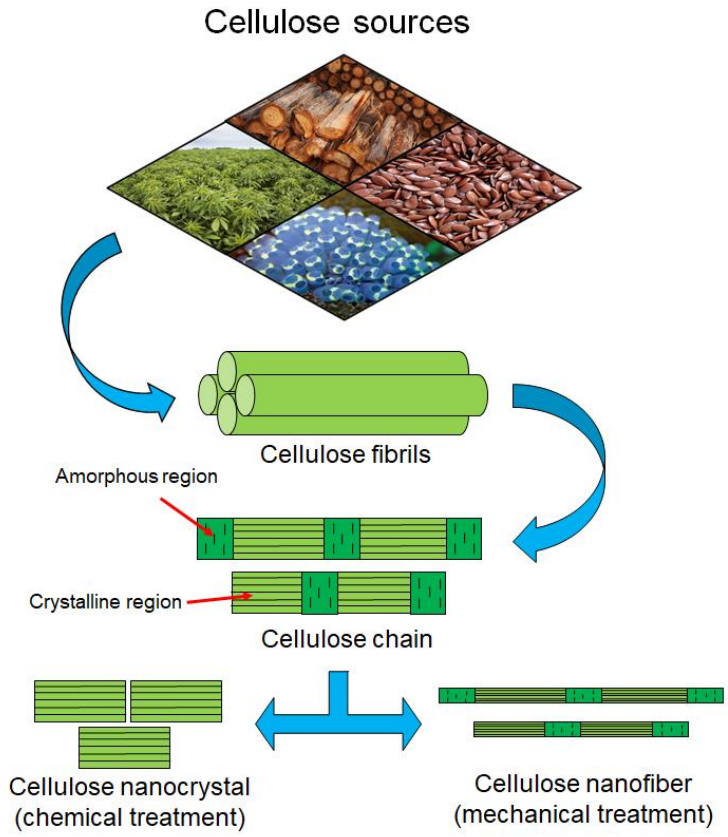

Figure 2. Extraction of nanocellulose from its sources.

Mechanical and chemical treatments are among the methods used to extract or produce nanocellulose from its sources. One of the mechanical treatments, high-pressure homogenization, is used for higher uniformity size distribution. This method is used by forcing the raw cellulose to pass through a very narrow channel using a pressurized piston (50–2000 MPa).[20] Also, this method is environmentally friendly for isolation.[21] However, there is a possibility that this procedure could cause the crystalline structure of cellulose to be damaged.[22] Another environmentally friendly method is a stone grinding technique in which cellulose is dispersed in water prior to the fibrillation. The stone grinder is rotated by about 1500 rpm, which applied shear stress on the cellulose and break down the size of fiber into nanoscale.[23] Water evaporation occurs as a result of the frictional

heat during the grinding process, which also enhances the extraction process.[24] Another method to extract cellulose fiber is the crushing technique, in which the fiber is frozen before crushed into smaller size cellulose.[25] The size of the cellulose generated varies between 0.1 and 1 μm. This method can be used as a pretreatment before high-pressure homogenization to produce nanocellulose.

Nanocellulose-based materials as sustainable bionanomaterial are non-toxic, recyclable, sustainable, and carbon-neutral.[26] CNF and CNC have shown a various range of innovative applications, including aerospace, optically translucent fabrics, drug delivery, coating films, tissue technology, biomimetic products, aerogels, sensors, three-dimensional (3D) printing, rheology modifiers, energy harvesters, filtration, textiles, printed and flexible plastics, composites, paper and board, packaging, oil and gas, medical and healthcare, and scaffolding.[27,28] Due to its highly abundant in nature with high mechanical strength and biodegradability, cellulose can be also used as a filler for polymer composites.[29] For instance, 48% improvement was achieved for the storage modulus of poly(vinyl alcohol) (PVA) and CNF composites.[30] Besides CNF, CNC possessed high mechanical strength as well and had been studied widely as composites with several polymers such as polyurethane (PU), poly (ε-caprolactone) (PCL), poly(ethylene glycol) (PEG), polystyrene (PS), and polypropylene (PP).[31–34] Another example of cellulose as a filler is the research on the different effects between CNC and CNF fillers against natural rubber.[35] Also, cellulose fibers can be used as an alternative for synthetic fibers, which are irritating, non-recyclable, and corrosive.[36] Generally, cellulose filler will improve the chemical or physical properties of polymer composites. The combination of cellulose filler and polymer matrix may produce a material with enhanced characteristics, which differs from a neat polymer matrix. Conducted researches proved that nanocellulose increased the tensile strength and thermal conductivity of synthetic polymers and bio-based polymers. **Table 1** shows examples of cellulose composites with their polymers matrices.

Table 1. Examples of polymer composites with cellulose as reinforcing materials.

Cellulose sources	Type of polymers as matrix	References
Microcrystalline cellulose	Poly(lactic acid)	[37]
Microcrystalline cellulose	Poly(butylene succinate)/poly(lactic acid)	[38]
Tunicin	Epoxy	[39]
Nata-de-coco	Poly(lactic acid) 213,241	[40,41]
Wood cellulose pulps	Chitosan 248	[42]
Cotton cellulose powder	Plasticized starch 171	[43]
Cellulose nanofiber	poly(3-hydroxybutyrate-co-3-hydroxyvalerate)	[44]
Cellulose nanocrystal	Poly(butylene succinate)	[45]
Cellulose nanocrystal	Poly(hydroxyl acid)-poly(lactic acid) 220	[46]

However, the compatibility between CNF and the hydrophobic polymer is generally quite low due to their different interaction with water molecules. CNF is required to be modified before composite preparation with hydrophobic polymer matrices such as poly(lactic acid) (PLA) or poly(methyl methacrylate) (PMMA). In recent decades, various transparent polymers have gained attention because of their excellent optical clarity such as PMMA. PMMA is often used as a substitute for glass material because of its high mechanical-dynamical properties and optical transparency. However, the applications of PMMA are limited owing to its insufficient mechanical strength and impact resistance, which limit its efficiency in engineering applications.[47] Therefore, some researches have been conducted to overcome these limitations by preparing composites of PMMA via reinforcement with nano- and micro-sized fibers.[48–50] In its natural form, bio-based poly(lactic acid) (PLA) features a transparent polymer too. Nowadays, transparent PLA pellets or

filaments can be produced by several methods and it is commercially available. In industry, PLA is currently commercialized as single-use disposal packaging.[51] However, PLA has several drawbacks that limit its applications, such as low thermal, mechanical, and barrier properties.[52] Therefore, many researches have been carried out to enhance and counter these drawbacks by preparing PLA composites.[53] Cellulose is a great candidate as a filler to counter the drawbacks of PMMA due to its high mechanical strength and biodegradability.[29]

The nature of cellulose by having high crystallinity and several hydrogen bonds in between/within its molecules is the main reason why it is difficult to be dissolved in water and organic solvents (**Figure 3**). Depends on the applications, this is one of the drawbacks of the utilization of cellulose. Therefore, cellulose modification gains high interest to counter this problem. A single unit of cellulose has three active hydroxyl groups. These groups can easily form hydrogen bonds, resulting in cellulose showing hydrophilicity. Most researchers manipulated these hydroxyl groups into a series of derivatization reactions, such as etherification, esterification, crosslinking, graft copolymerization, etc.[54] **Table 2** exhibits some examples of modified-cellulose.

Esterification of cellulose is a process of involving the hydroxyl groups in the glucose unit of cellulose with organic acid including carboxylic acid or acid anhydride, which produces water as a side product.[55] According to the previous research, cellulose can be esterified by several organic acids such as fatty acid (anhydride) with various carbon chain lengths. Several examples of cellulose modified with acid anhydrides are the modification with formic acid,[56] acetic anhydride,[57] propionic anhydride,[58] butyric anhydride,[59] and valeric acid.[60] The esterified cellulose will change the nature of cellulose into hydrophobic species due to the substitution of the hydrophobic group on its hydroxyl groups. Esterified cellulose can be utilized as composites material and have higher compatibility with hydrophobic polymer matrix compared to pristine cellulose.

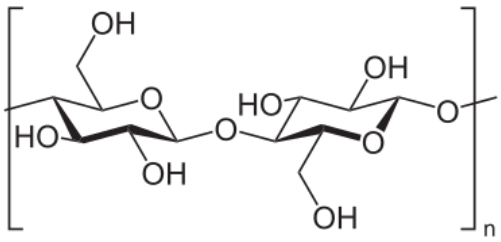

Figure 3. Chemical structure of cellulose.

Table 1. Examples of polymer composites with cellulose for various applications.

Modified cellulose	Cellulose sources	References
TEMPO-oxidized	Cellulose nanofiber	[61]
Anionic surfactant	Bacterial cellulose	[54]
Etherification	Microcrystalline cellulose	[60]
Carboxylated	Cellulose nanofiber	[62]
Polymerized methyl methacrylate	Cellulose nanofiber	[63]
Acetylated	Cellulose nanofiber	[57]
Butyrylated	Cellulose nanofiber	[59]
Acylated	Bacterial cellulose	[64]

Thesis Contents

Chapter 1 – Acetylation of Fibrillated Cellulose Nanofiber by Acetic Anhydride as Filler in Poly(lactic acid) Composite Films

In this chapter, the efficiency of PLA when CNF (before and after modification) is added as a filler. When compared to conventional methods such as 2,2,6,6-tetramethylpiperidine-1-oxyl (TEMPO) oxidation, CNF developed by green fibrillation process without any chemical pre-treatment had advantages in terms of low cost and time-saving. It was demonstrated that the substitution of CNF's hydroxyl group into acetyl group changed the compatibility of m-CNF with the PLA matrix. Acetylated cellulose nanofiber (CNFa) and PLA formed smooth surface composite films with good transparency and mechanical properties (**Figure 4**). Moreover, the tensile strength of neat PLA film was improved when CNFa was used as the filler. Furthermore, without lowering the thermal stability of PLA, composite films of PLA/CNFa exhibited lower wettability compared with that of neat PLA film.

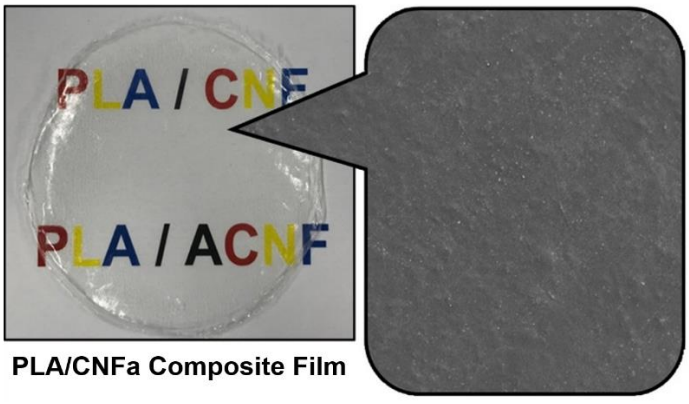

Figure 4. Good compatibility between CNFa filler and PLA matrix.[57]

Chapter 2 – Effects of Acid Anhydrides-Modified Cellulose Nanofiber on Poly(lactic acid) Composite Films

In this chapter, the effect of the addition of CNF fillers on the performance of PLA was studied. Substitution of the hydroxyl group of cellulose to the acyl group by acid anhydrides changed the compatibility of the CNF with PLA. CNF was modified by acetic anhydride (AA), propionic anhydride (PA), and butyric anhydride (BA) to form surface-modified CNFa, propionylated CNF (CNFp), and butyrylated CNF (CNFb), respectively, to improve the compatibility with the PLA matrix. The effects of the different acid anhydrides were compared based on their rates of reaction in the acylation process. PLA with modified CNF (m-CNF) fillers formed smoother surfaces with better transparency, mechanical, and wettability properties compared with the PLA/CNF composite film. The effects of CNFa, CNFp, and CNFb on the PLA matrix were compared (**Figure 6**), and it was found that CNFp was the best filler for PLA.

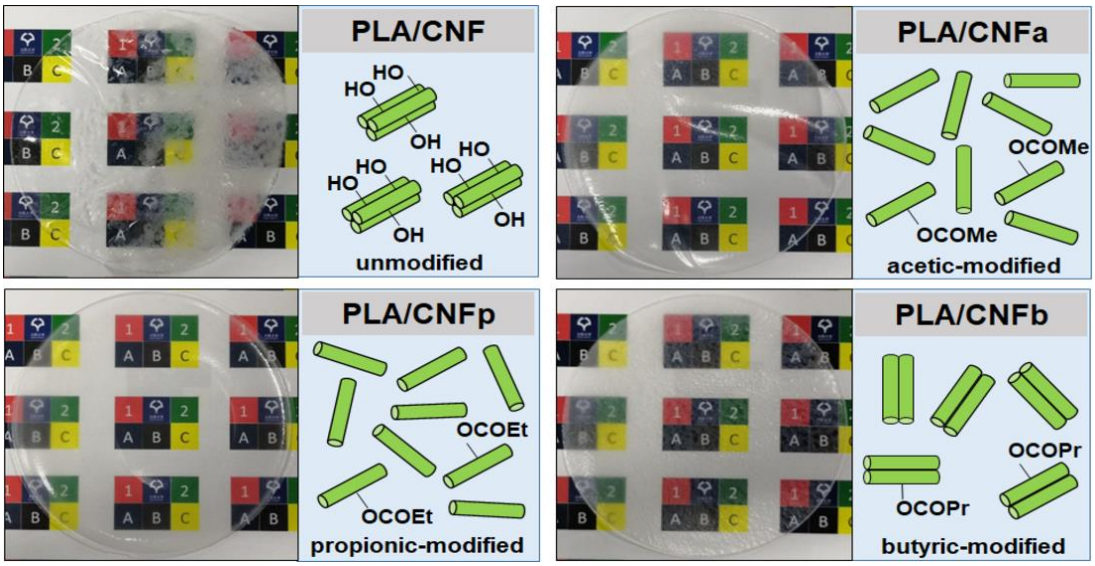

Figure 5. Comparison among CNF, CNFa, CNFp and CNFb as fillers on the transparency of PLA composite films.[59]

Chapter 3 – Acylation of Cellulose Nanofiber as Filler for Poly(methyl methacrylate) Composite Films

In this chapter, the compatibility of m-CNFs filler and PMMA matrix was studied instead of PLA matrix (previous chapters) (**Figure 6**). CNF, CNFp, and CNFa were compared with respect to their influence as fillers in PMMA composite films by ultraviolet−visible (UV) transmittance, haze values, tensile strength testing, and water contact angle (WCA) measurement. It was demonstrated that CNFp has good compatibility and uniform dispersion in the PMMA matrix, as evidenced by the formation of a smooth surface composite film with good transparency, enhanced tensile properties, improved toughness, and lower wettability. Therefore, PMMA/CNFp composite films have great potential for use in several applications such as lightweight transparent materials, window substitutes, and see-through packaging.

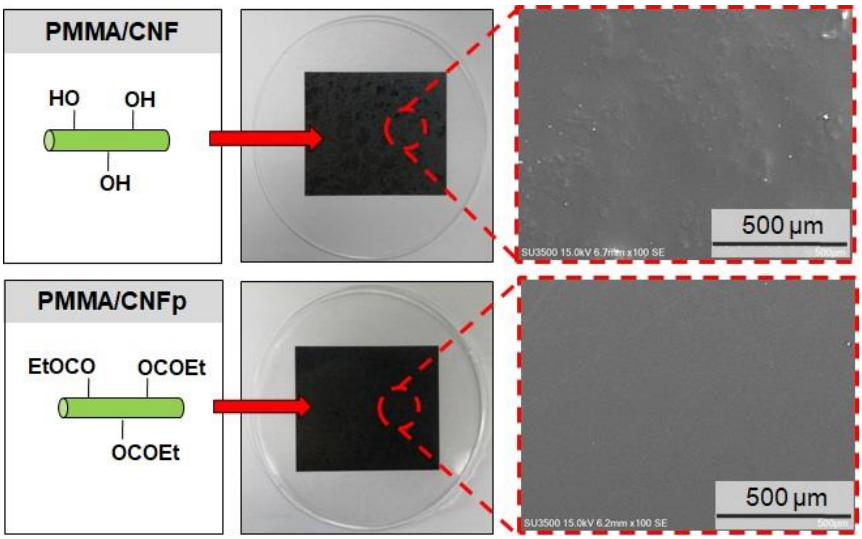

Figure 6. Comparison between CNF and CNFp as fillers in PMMA composite films.[58]

References

1 A. L. Andrady and M. A. Neal, *Philos. Trans. R. Soc. B Biol. Sci.*, 2009, **364**, 1977–1984.

2 E. L. Teuten, J. M. Saquing, D. R. U. Knappe, M. A. Barlaz, S. Jonsson, A. Björn, S. J. Rowland, R. C. Thompson, T. S. Galloway, R. Yamashita, D. Ochi, Y. Watanuki, C. Moore, P. H. Viet, T. S. Tana, M. Prudente, R. Boonyatumanond, M. P. Zakaria, K. Akkhavong, Y. Ogata, H. Hirai, S. Iwasa, K. Mizukawa, Y. Hagino, A. Imamura, M. Saha and H. Takada, *Philos. Trans. R. Soc. B Biol. Sci.*, 2009, **364**, 2027–2045.

3 R. C. Thompson, C. J. Moore, F. S. V. Saal and S. H. Swan, *Philos. Trans. R. Soc. B Biol. Sci.*, 2009, 364, 2153–2166.

4 R. J. Moon, A. Martini, J. Nairn, J. Simonsen and J. Youngblood, *Chem. Soc. Rev.*, 2011, **40**, 3941–3994.

5 S. Wang, A. Lu and L. Zhang, *Prog. Polym. Sci.*, 2016, 53, 169–206.

6 X. Huang and A. Netravali, *Compos. Sci. Technol.*, 2009, **69**, 1009–1015.

7 D. Klemm, B. Heublein, H. P. Fink and A. Bohn, *Angew. Chemie - Int. Ed.*, 2005, 44, 3358–3393.

8 Q. Xu, C. Chen, K. Rosswurm, T. Yao and S. Janaswamy, *Carbohydr. Polym.*, 2016, **149**, 274–281.

9 T. Abitbol, A. Rivkin, Y. Cao, Y. Nevo, E. Abraham, T. Ben-Shalom, S. Lapidot and O. Shoseyov, *Curr. Opin. Biotechnol.*, 2016, 39, 76–88.

10 D. Klemm, E. D. Cranston, D. Fischer, M. Gama, S. A. Kedzior, D. Kralisch, F. Kramer, T. Kondo, T. Lindström, S. Nietzsche, K. Petzold-Welcke and F. Rauchfuß, *Mater. Today*, 2018, 21, 720–748.

11 L. Thompson, J. Azadmanjiri, M. Nikzad, I. Sbarski, J. Wang and A. Yu, *Rev. Adv. Mater.*

Sci., 2019, **58**, 1–16.

12 C. J. Chirayil, J. Joy, L. Mathew, M. Mozetic, J. Koetz and S. Thomas, *Ind. Crops Prod.*, 2014, **59**, 27–34.

13 S. Shankar and J. W. Rhim, *Carbohydr. Polym.*, 2016, **135**, 18–26.

14 M. T. Islam, M. M. Alam, A. Patrucco, A. Montarsolo and M. Zoccola, *AATCC J. Res.*, 2014, 1, 17–23.

15 V. Kumar, R. Bollström, A. Yang, Q. Chen, G. Chen, P. Salminen, D. Bousfield and M. Toivakka, *Cellulose*, 2014, **21**, 3443–3456.

16 G. Siqueira, J. Bras and A. Dufresne, *Polymers (Basel).*, 2010, 2, 728–765.

17 N. Lavoine, I. Desloges, C. Sillard and J. Bras, *Cellulose*, 2014, **21**, 4429–4442.

18 L. Brinchi, F. Cotana, E. Fortunati and J. M. Kenny, *Carbohydr. Polym.*, 2013, 94, 154–169.

19 V. C. Santos-Ebinuma, I. C. Roberto, M. F. Simas Teixeira and A. Pessoa, *Biotechnol. Prog.*, 2013, **29**, 778–785.

20 H. Kargarzadeh, M. Ioelovich, I. Ahmad, S. Thomas and A. Dufresne, in *Handbook of Nanocellulose and Cellulose Nanocomposites*, Wiley-VCH Verlag GmbH & Co. KGaA, 2017, pp. 1–49.

21 K. Saelee, N. Yingkamhaeng, T. Nimchua and P. Sukyai, *Ind. Crops Prod.*, 2016, **82**, 149–160.

22 S. Rebouillat and F. Pla, *J. Biomater. Nanobiotechnol.*, 2013, **04**, 165–188.

23 I. Siró and D. Plackett, *Cellulose*, 2010, 17, 459–494.

24 M. Jonoobi, J. Harun, P. M. Tahir, L. H. Zaini, S. SaifulAzry and M. D. Makinejad, *BioResources*, 2010, **5**, 2556–2566.

25 A. Alemdar and M. Sain, *Bioresour. Technol.*, 2008, **99**, 1664–1671.

26 A. Dufresne, *Mater. Today*, 2013, 16, 220–227.

27 F. V. Ferreira, C. G. Otoni, K. J. De France, H. S. Barud, L. M. F. Lona, E. D. Cranston and O. J. Rojas, *Mater. Today*, 2020, 37, 126–141.

28 F. Ansari, Y. Ding, L. A. Berglund and R. H. Dauskardt, *ACS Nano*, 2018, **12**, 5495–5503.

29 A. Shalwan and B. F. Yousif, *Mater. Des.*, 2013, **48**, 14–24.

30 Y. Oishi, M. Nakaya, E. Matsui and A. Hotta, *Compos. Part A Appl. Sci. Manuf.*, 2015, **73**, 72–79.

31 A. Pei, J. M. Malho, J. Ruokolainen, Q. Zhou and L. A. Berglund, *Macromolecules*, 2011, **44**, 4422–4427.

32 A. L. Goffin, J. M. Raquez, E. Duquesne, G. Siqueira, Y. Habibi, A. Dufresne and P. Dubois, *Polymer (Guildf).*, 2011, **52**, 1532–1538.

33 N. Lin and A. Dufresne, *Macromolecules*, 2013, **46**, 5570–5583.

34 S. Iwamoto, S. Yamamoto, S. H. Lee and T. Endo, *Compos. Part A Appl. Sci. Manuf.*, 2014, **59**, 26–29.

35 A. Bendahou, H. Kaddami and A. Dufresne, *Eur. Polym. J.*, 2010, **46**, 609–620.

36 P. Wambua, J. Ivens and I. Verpoest, *Compos. Sci. Technol.*, 2003, **63**, 1259–1264.

37 R. D. Kale, V. G. Gorade, N. Madye, B. Chaudhary, P. S. Bangde and P. P. Dandekar, *Int. J. Biol. Macromol.*, 2018, **118**, 1090–1102.

38 X. Zhang and Y. Zhang, *Carbohydr. Polym.*, 2016, **140**, 374–382.

39 S. Xu, N. Girouard, G. Schueneman, M. L. Shofner and J. C. Meredith, *Polymer (Guildf).*, 2013, **54**, 6589–6598.

40 J. J. Blaker, K. Y. Lee, M. Walters, M. Drouet and A. Bismarck, *React. Funct. Polym.*, 2014, **85**, 185–192.

41 M. Hervy, J. J. Blaker, A. L. Braz and K. Y. Lee, *Compos. Part A Appl. Sci. Manuf.*, 2018,

107, 155–163.

42 Y. Wang, K. Uetani, S. Liu, X. Zhang, Y. Wang, P. Lu, T. Wei, Z. Fan, J. Shen, H. Yu, S. Li, Q. Zhang, Q. Li, J. Fan, N. Yang, Q. Wang, Y. Liu, J. Cao, J. Li and W. Chen, *ChemNanoMat*, 2017, **3**, 98–108.

43 S. Yang, Y. Tang, J. Wang, F. Kong and J. Zhang, *Ind. Eng. Chem. Res.*, 2014, **53**, 13980–13988.

44 Y. Srithep, T. Ellingham, J. Peng, R. Sabo, C. Clemons, L. S. Turng and S. Pilla, *Polym. Degrad. Stab.*, 2013, **98**, 1439–1449.

45 J. Xu, P. H. Manepalli, L. Zhu, S. Narayan-Sarathy and S. Alavi, *J. Polym. Res.*, 2019, **26**, 1–10.

46 G. Mármol, C. Gauss and R. Fangueiro, *Molecules*, 2020, **25**, 4653.

47 H. Liu, D. Liu, F. Yao and Q. Wu, *Bioresour. Technol.*, 2010, **101**, 5685–5692.

48 R. J. Nussbaumer, W. R. Caseri, P. Smith and T. Tervoort, *Macromol. Mater. Eng.*, 2003, **288**, 44–49.

49 L.-S. Chen, Z.-M. Huang, G.-H. Dong, C.-L. He, L. Liu, Y.-Y. Hu and Y. Li, *Polym. Compos.*, 2009, **30**, 239–247.

50 E. Tang, G. Cheng and X. Ma, *Powder Technol.*, 2006, **161**, 209–214.

51 Y. Bor, J. Alin and M. Hakkarainen, *Packag. Technol. Sci.*, 2012, **25**, 427–433.

52 M. Murariu and P. Dubois, *Adv. Drug Deliv. Rev.*, 2016, 107, 17–46.

53 M. P. Arrieta and L. Peponi, *Eur. Polym. J.*, 2017, **89**, 174–184.

54 J. C. Courtenay, M. A. Johns, F. Galembeck, C. Deneke, E. M. Lanzoni, C. A. Costa, J. L. Scott and R. I. Sharma, *Cellulose*, 2017, **24**, 253–267.

55 Y. Cao, H. Li and J. Zhang, *Ind. Eng. Chem. Res.*, 2011, **50**, 7808–7814.

56 P. Willberg-Keyriläinen, J. Vartiainen, J. Pelto and J. Ropponen, *Carbohydr. Polym.*, 2017,

170, 160–165.

57 N. Jamaluddin, T. Kanno, T. A. Asoh and H. Uyama, *Mater. Today Commun.*, 2019, **21**, 100587.

58 N. Jamaluddin, Y. I. Hsu, T. A. Asoh and H. Uyama, *ACS Omega*, 2021, **6**, 10752–10758.

59 N. Jamaluddin, Y. I. Hsu, T. A. Asoh and H. Uyama, *Nanomaterials*, 2021, **11**, 1–15.

60 Y. Dong, L. I. Mosquera-Giraldo, L. S. Taylor and K. J. Edgar, *Biomacromolecules*, 2016, **17**, 454–465.

61 S. Fujisawa, T. Saito, S. Kimura, T. Iwata and A. Isogai, *Biomacromolecules*, 2013, **14**, 1541–1546.

62 H. Dong, Y. R. Sliozberg, J. F. Snyder, J. Steele, T. L. Chantawansri, J. A. Orlicki, S. D. Walck, R. S. Reiner and A. W. Rudie, *ACS Appl. Mater. Interfaces*, 2015, **7**, 25464–25472.

63 Y. F. Shih, M. Y. Chou, H. Y. Lian, L. R. Hsu and S. M. Chen-Wei, *Express Polym. Lett.*, 2018, **12**, 844–854.

64 C. Qian, T. A. Asoh and H. Uyama, *Chem. Commun.*, 2018, **54**, 11320–11323.

Chapter 1

Acetylation of Fibrillated Cellulose Nanofiber by Acetic Anhydride as Filler in Poly(lactic acid) Composite Films

1.1 Introduction

Nowadays, bio-based polymers have attracted much attention as the substitute for current materials such as synthetic plastics and petroleum-based materials. The utilization of bio-based polymers is the key factor for developing a sustainable society because of its renewability and biocompatibility, which will reduce plastic waste. One of the bio-based polymers is PLA, which has the most interesting features compared with others because of its sufficient ability to process, transparency, and crystallinity.[1] PLA is a flexible material that can possess several characteristics depending on its processing condition such as high or low crystallinity to form either opaque or transparent material. Also, its molecular weight is varying depending on the starting process method, which gives sufficient or low physical properties. Current PLAs are already commercialized in industries as single-used disposal packaging applications.[2] However, applications of PLA are limited due to its low thermal, mechanical, and barrier properties.[3] Therefore, several types of research have been conducted to improve these limitations by preparing composites of PLA.[4] Biopolymer nanocomposite of PLA/cellulose is expected to show superior properties by the combination of plastic matrix and cellulose filler.

Acetylation on cellulose has been widely conducted to substitute the hydroxyl group of cellulose to form the acetyl group. This modification can alter its hydrophilicity, which can prevent the wetting behavior of cellulose and improve its thermal stability.[5] For example, Jonoobi et al. (2012) stated that the surface modification by acetylation showed improvement of cellulose hydrophobicity, which enhanced the dispersibility in hydrophobic polymers.[6]

There are several types of research to modify CNFs by functionalizing with acetylation and silylation through reactions with anhydrous acetic acid and *n*-dodecyldimethylchlorosilane, respectively.[5,7] Another famous technique of cellulose functionalization is the use of TEMPO oxidation on the hydroxyl group of cellulose, which was mentioned earlier.[8] Several other modifications of cellulose had been deliberated such as esterification on BC, alkylation on micro- and nanocellulose, silanization by 3-methacrysloxypropyltrimethoxysilane (MEMO), and glyoxalization process on BC networks.[9–12] Thus, various functionalization of cellulose was made to enhance the compatibility of cellulose with the chosen polymer matrix.

In this chapter, microcrystalline cellulose (MCC) was ground by a stone grinding machine without any chemical treatment to prepare micro-scale to nanoscale cellulose fibers. Then, surface modification toward the hydroxyl group was conducted by AA to form CNFa. The impact of CNFa as a filler was observed in PLA composite films. Moreover, the comparison between CNF and CNFa to act as fillers toward PLA were explained in this study focusing on their physical property such as tensile strength and transparency. Also, the compatibility of PLA matrix with fillers was presented by surface morphology from scanning electron microscope (SEM).

1.2 Experimental section

1.2.1 Materials

MCC was obtained from MERCK Japan Ltd. (Tokyo, Japan). N,N-dimethylformamide (DMF) was purchased from Kanto Chemical (Tokyo, Japan). AA, cellulose acetate (CA), chloroform >99.0%, and acetone >99.0% were obtained from Wako Pure Chemical Industries (Osaka, Japan) and used without treatment. PLA (PLA2003D Ingeo biopolymer) was purchased from NatureWorks LLC (Minnesota, MN, USA).

1.2.2 Fibrillation of MCC

Fibrillation of MCC was performed with a stone grinding machine (Masuko Sangyo, Saitama, Japan) without other chemical treatments. In brief, MCC (40 g) was soaked and stirred in 2 L water for 2 days to produce a suspension of 2 wt% MCC. The MCC suspension was then ground at 1500 rpm for 10 cycles with a stone grinder grit size of 80 (ultra-fine). As the fiber size decreased, MCC automatically exited the chute in the form of CNF. Each cycle was repeated when the hopper was almost empty by transferring the product of the previous cycle back into the hopper. Procedures were repeated *x* times to obtain CNF with the smaller size and samples produced were denoted based on their cycles as *x*-CNF. **Figure 1-1** illustrated the process of grinding fibrillation of MCC.

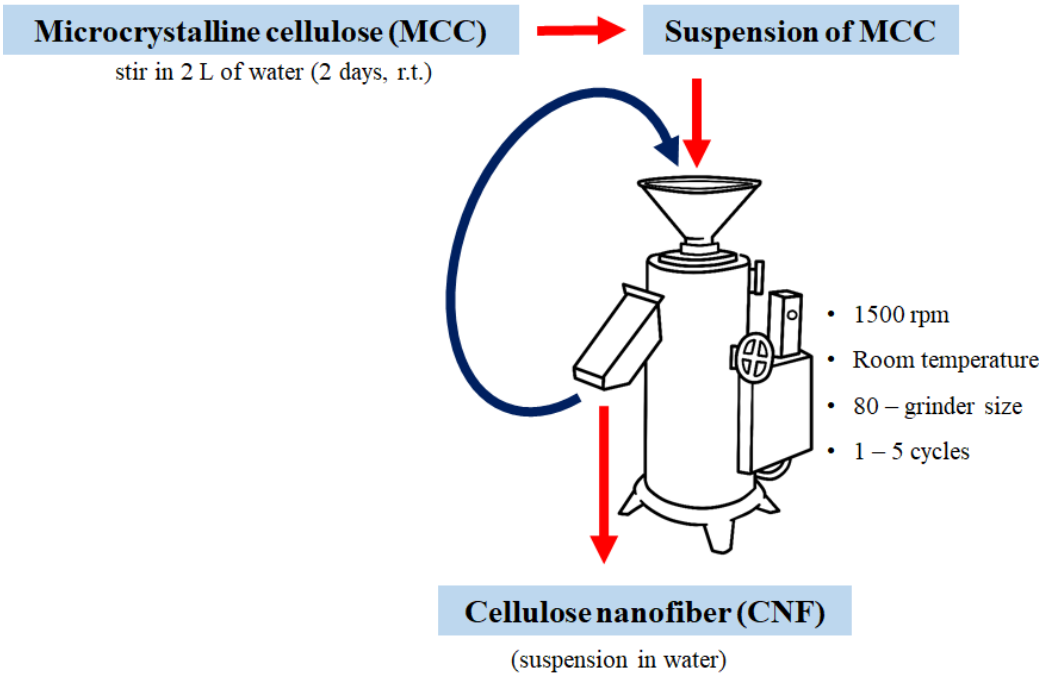

Figure 1-1. Grinding fibrillation of MCC to produced CNF.

1.2.3 Surface Modification of CNF

The concept of the acetylation process was inspired by Bulota and Hughes (2012).[13] First, 10 g of CNF in water (2.5 wt%) was diluted with 40 mL of another water before sonication. Next, DMF (80 mL) was added and the suspension was stirred at room temperature for 15 minutes. The suspension of CNF in mixed solvent was transferred in a rotary evaporator. Then, water was further removed by heating at 110 °C for 1 hour with stirring. Next, AA (25–75 g) was added and the heating process was continued for another 1–20 hours. The solution then was quenched in an ice bath followed by adding acetone (60 mL). After that, the solution was centrifuged twice with sufficient acetone to wash the solvents. Finally, the medium was exchanged with chloroform to obtained acetylated cellulose nanofiber (CNFa) in chloroform.

1.2.4 Preparation of PLA Composite Films

The **s**olution casting method was used to prepare PLA composites. First, CNF (or CNFa), PLA, and chloroform were mixed in a round bottom flask and refluxed simultaneously (one-pot reaction) at 50 °C with stirring. Then, the solution was poured on a petri dish and left overnight in a bio shaker with 25 rpm and 25 °C to evaporate the chloroform. The sample was denoted as PLA/CNF or PLA/CNFa.

1.2.5 Characterizations

The microstructure of CNF and their composites were observed by an SEM instrument (SU3500, Hitachi, Tokyo, Japan) using Au–Pd sputter. Also, SEM was used to calculate the fibers' diameter by measuring the wide of at least 30 specimens, which were picked randomly among the fibers in captured images. Attenuated total reflection infrared (ATR-IR) instrument (iD5 ATR, Thermo Scientific, Waltham, MA, USA) was used to observe functional groups after modification. ATR-IR was used for the calculation of the degree of substitution (DS) of CNFa as well. Fei's method was followed by comparing the area of acetyl group vibration ($\nu_{C=O}$) around 1730 cm^{-1} and

an area of C-O-C peak (the backbone of anhydroglucose) at1180–920 cm^{-1}.[14] The intensity of the C-O-C peak around 1050 cm^{-1} remained the same after acetylation because it did not participate in the reaction. Commercialized CA was used as a reference for the DS calculation of CNFa. The transmittances of composite films were elucidated by UV and visible light spectrophotometer (UV-Vis) (U-2810 spectrophotometer, Hitachi, Tokyo, Japan) under visible region (200–800 nm) with a rate of 800 nm/min. The crystallinities of PLA composites were calculated using differential scanning calorimetry (DSC) (EXSTAR 6000 DSC6220, SEIKO, Tokyo, Japan) from crystallization temperature (T_c) and melting temperature (T_m) areas. The crystallinities of the PLA composite films were calculated using the theoretical heat of fusion ($\Delta \boldsymbol{H_f}$) (93.1 J g^{-1}) as shown in **equation 1-1** and **1-2**.[15]

$$\Delta \boldsymbol{Hm} - \Delta \boldsymbol{Hc} = \Delta \boldsymbol{H'} \textbf{ (Equation 1-1)}$$

$$\frac{\Delta \boldsymbol{H'}}{\Delta \boldsymbol{Hf}} \textbf{ x } \boldsymbol{100 = X_c} \textbf{ \% (Equation 1-2)}$$

$$\Delta \boldsymbol{H_f} \textbf{ = 93.1 J/g}$$

where, $\Delta \boldsymbol{H_m}$ and $\Delta \boldsymbol{H_c}$ are the enthalpies given during melting and crystallization, respectively, and X_c % is the degree of crystallinity.

The mechanical properties of the composite films were investigated by Universal Testing Machine (EZ Graph, Shimadzu, Kyoto, Japan). Every sample was cut into dumbbell shape for at least 8 specimens and dried in the oven at 80 °C before analysis to remove the remaining solvent. The samples were stretched at 5 mm/s with 100 N load and samples after the tensile test were then further characterized by SEM, observing the breaking point area. Thermal decompositions of the PLA composites were measured using thermogravimetry analysis (TGA) machine (EXSTAR 6000 TG/DTA7200 standard type, SEIKO, Tokyo, Japan) at the rate of 10 °C/min from 50 °C to 550 °C. All films were dried overnight using a vacuum oven at 40°C before the thermal analysis.

Hydrophobicity of the films was studied with a WCA test by contact angle measurement instrument (Drop Master DM300, Kyowa Interface Science, Tokyo, Japan), with FAMAS basic software. Every sample was measured for at least 5 specimens to calculate the average contact angle.

1.3 Results and discussion

1.3.1 Stone Grinding of MCC

Cellulose with finer fibers size was produced with increasing grind cycle (**Figure 1-2**). A clear difference in size was found for MCC before and after grinding fibrillation, with 3-CNF showed no obvious agglomeration. Moreover, the fibers sizes of 5-CNF were slightly smaller compared with 3-CNF. The average diameter of 3-CNF was 93 ± 28 nm, which is in the nanoscale region. The average diameter of 5-CNF was further reduced to 69 ± 21 nm. The standard deviations were calculated by 30 random fibers within the same SEM images. The previous study by Siró and Plackett indicated that finer cellulose size can be produced by increasing the number of grind cycles, however, its mechanical properties are weakened at the same time.[16] Therefore, five grind cycles were convenient as the CNF with smaller and finer fibers compared with 3-CNF can be obtained.

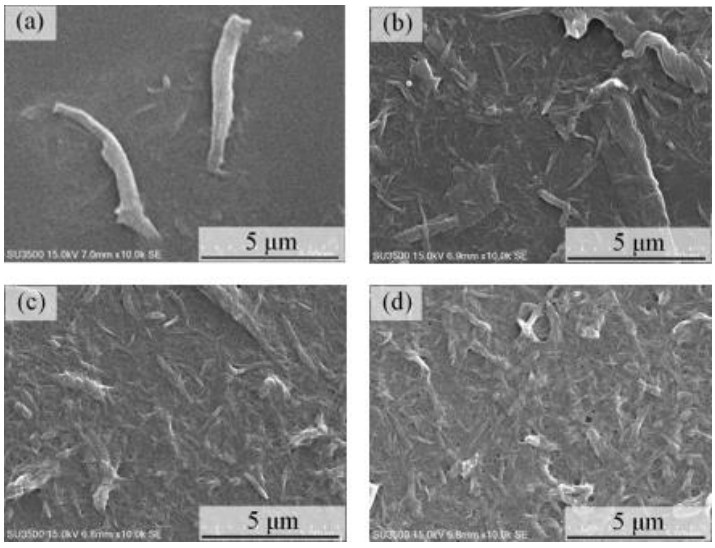

Figure 1-2. SEM images of (a) MCC, (b) 1-CNF, (c) 3-CNF and (d) 5-CNF.

1.3.2 Surface Modification of CNF

ATR-IR was used to observe the differences and changes in the functional group after acetylation of CNF by the AA. **Figure 1-3** shows that acetyl peak appeared on the ATR-IR spectrogram for all CNFa products, and the DS value of CNFa based on their reaction parameters were summarized in **Table 1-1**. CNFs were reacted with 75 g and 50 g AA for 4 hours to study the acetylation at lower reaction time which resulted in DS of 1.07 and 0.75, respectively. CA was used as a reference during the calculation of the DS. It was demonstrated that the reaction with 75 g AA showed a high acetylation rate comparable with that of 20 hours (DS = 1.15). Therefore, acetylation of CNF was optimized at 4 hours with lower energy instead of 20 hours with the same amount of AA. Throughout this study, acetylated CNF with an optimized condition (DS = 1.07) was used for composite preparation with PLA composites.

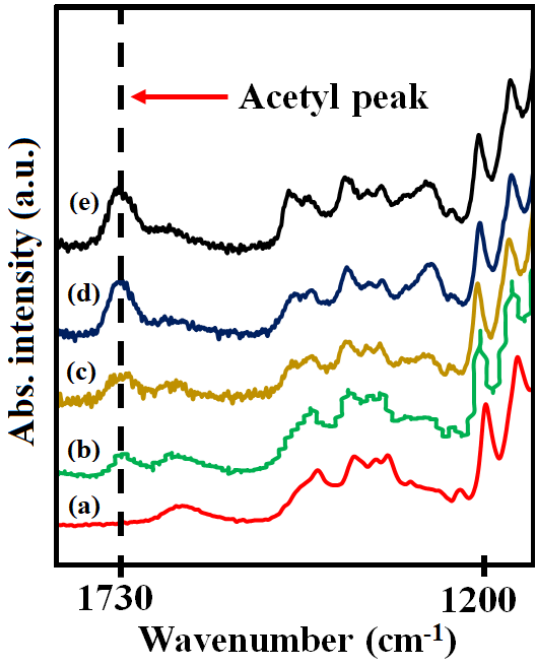

Figure 1-3. ATR-IR spectrograms for (a) MCC and CNFa with different reaction time and amount of AA used, where, (b) 1 h, 25 g; (c) 4 h, 50 g; (d) 4 h, 75 g; and (e) 20 h, 75 g.

Table 1-1. Value of DS of CNFa based on their reaction time and amount of AA used.

Reaction time (hours)	Amount of AA used (g)	DS value
1	25	0.62
4	50	0.75
4	75	1.07
20	75	1.15

*DS was calculated by comparing the area of acetyl group vibration (*ν*C=O) and an area of C-O-C peak.

1.3.3 Appearances of m-CNFs

The appearances of CNF and CNFa solutions were much different while in chloroform because of their compatibility with the solvent. Illustrated in **Figure 1-4**, CNF in chloroform showed some permanent aggregation even after the sonication process for more than 10 minutes. Meanwhile, low degree CNFa showed some aggregation in the chloroform, however, after sonication, the dispersion was improved and continued to use for composite preparation with PLA. Moreover, a higher degree of acetylation showed different properties as it forms suspension-like behavior after leaving in the refrigerator for a certain period and the product dispersed well in chloroform after shook lightly for about 5 seconds. Another batch of high acetylation of CNFa in acetone showed precipitation after left in the refrigerator and dispersed well after shook lightly.

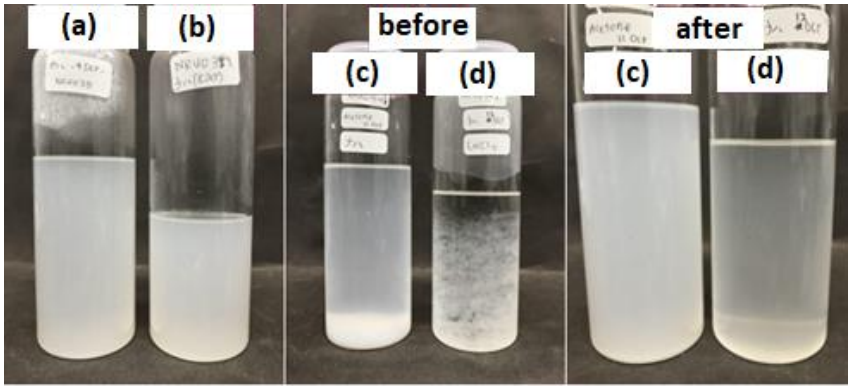

Figure 1-4. Appearance of (a) CNF, (b) low degree CNFa, (c) high degree CNFa in acetone, and (d) high degree CNFa in chloroform before and after shaking.

1.3.4 The Structure of CNF

Images from SEM were used to calculate the diameters of CNF and CNFa. A total of 30 specimens from each sample were measured to calculate the average diameter of CNFA in chloroform and acetone. It was confirmed that the average diameter of CNFa after the chemical modification was below 100 nm (**Figure 1-5**). The average diameters of CNFa fibers in solvents were maintained at 50 ± 8 and 72 ± 13 nm for chloroform and acetone, respectively. Both CNFA in chloroform and acetone exhibited nanoscale diameters without any significant agglomeration. In the meantime, the appearances of CNF and CNFa solutions were much different while in chloroform because of their compatibility with the solvent. CNF in chloroform showed some permanent aggregation even after the sonication process for more than 10 minutes. Meanwhile, CNFa with DS 0.62 showed some aggregation in the chloroform, however, after sonication, the dispersion was improved and continued to use for composite preparation with PLA. CNFa with DS 1.15 was dispersed well in chloroform after shook lightly because of the acetyl group substitution on the CNFa surface. Hence, increased its surface energy with PLA matrix.[17]

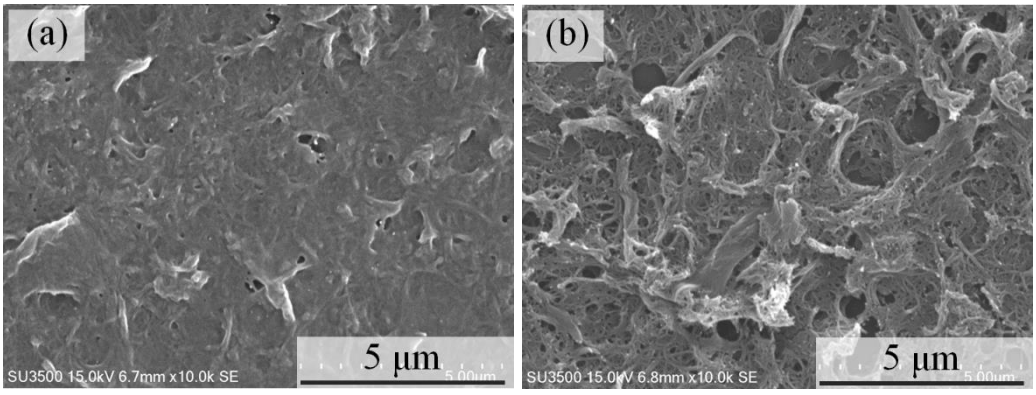

Figure 1-5. SEM images of (a) CNFa in acetone and (b) CNFa in chloroform.

1.3.5 Transparencies of PLA Composite Films

Composites of PLA with CNF and CNFa gave different physical properties especially on the surface because of the difference compatibility between the PLA matrix and its fillers. CNFa was expected to have high compatibility with PLA, while CNF was well known for its bad compatibility with PLA. Due to these reasons, the transparencies of the films were affected. As shown in **Figure 1-6**, all of the films possessed high transparencies when putting on the observation sheets. However, when the films were lifted 10 cm away from the sheet, the films started to show opacity due to the light scattering by the cellulose fibers. On the other hand, neat PLA film kept its transparency after lifted and the words are still clear as well as readable compared with the other films. The thicknesses of the films were calculated and summarized in **Table 1-2** to elucidate the effect on the physical properties and transparency. The thicknesses were ranged randomly from 0.012 mm (PLA/CNFa composite film) to 0.151 mm (PLA/CNF composite film), while neat PLA film had 0.125 mm thickness. Therefore, thicknesses did not affect the physical nor transparency properties of the films.

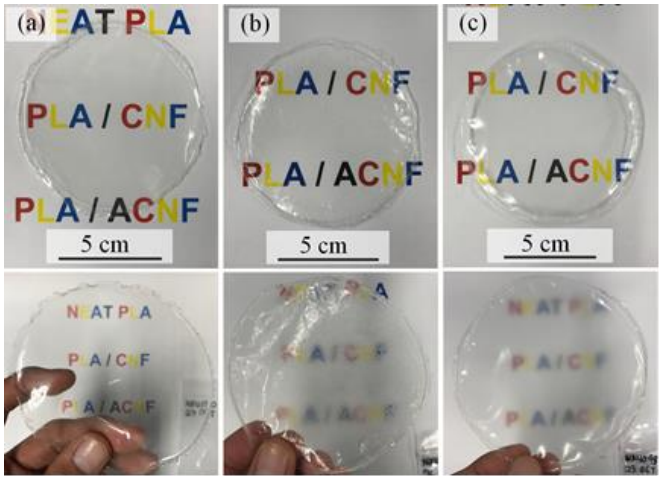

Figure 1-6. Optical properties of (a) neat PLA, (b) PLA/CNF, and (c) PLA/CNFa composite films (top = on sheet, bottom = 10 cm above from the sheet).

Table 1-2. The thicknesses for PLA composite films.

Composite films	Thickness (mm)
Neat PLA	0.125
PLA/CNF	0.151
PLA/CNFa	0.120

UV-Vis spectroscopy was carried out to support the comparison in transparency among PLA composite films by providing UV-Vis transmittance percentages (**Figure 1-7**). Neat PLA film showed 85% transmittance which was the highest among all PLA composite films. PLA/CNFa and PLA/CNF exhibited lower transmittances at 72% and 70%, respectively, due to the incorporation of cellulose fibers. Both PLA/CNFa and PLA/CNF composite films possessed almost similar transmittance, although PLA/CNFa composite films had 2% higher transmittance because of the good compatibility of CNFa.

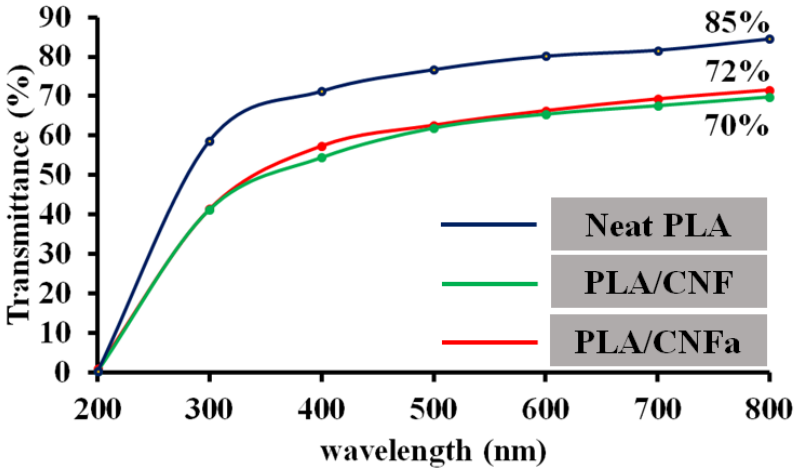

Figure 1-7. Differences in transmittance for all PLA composite films.

1.3.6 Compatibility of m-CNF with PLA Matrix

SEM was utilized to investigate the morphology of PLA composite films (**Figure 1-8).** It was observed that neat PLA had a smooth surface, whereas PLA/CNF1 and PLA/CNF2 showed clear CNF fibers. It is interesting to note that the larger CNF fibers appeared in PLA/CNF2 compared with PLA/CNF1. This is because CNF fibers started to agglomerate with an increased amount of filler due to the incompatibility with PLA. Meanwhile, CNFa was barely observed under the same magnification. From this result, it was demonstrated that acetylation on CNF changed the compatibility of cellulose with PLA. Thus, the agglomeration of cellulose fibers can be avoided by introducing the acetylated CNF instead of the unmodified CNF.

Also, cross-sections of the films were taken into account and normal plastic deformation on neat PLA films showed in **Figure 1-9**. It was in contrast with PLA/CNF composite film which had a more rigid structure. Meanwhile, flaky deformation was observed for PLA/CNFa composite film because CNFa acted as a plasticizer for PLA/CNFa composite film.

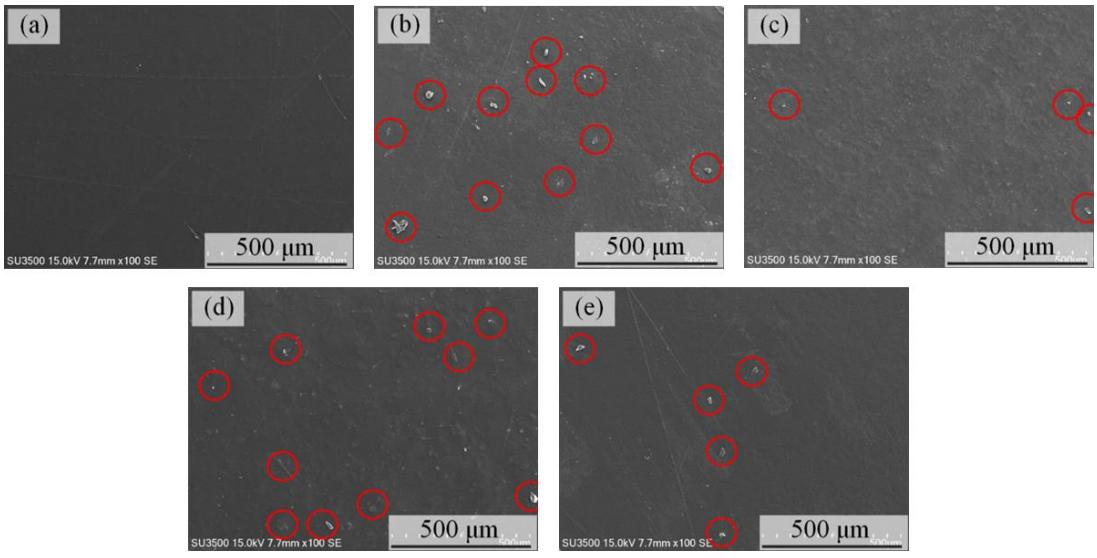

Figure 1-8. SEM images of (a) neat PLA, (b) PLA/CNF1, (c) PLA/CNFa1, (d) PLA/CNF2, and (e) PLA/CNFa2 composite films.

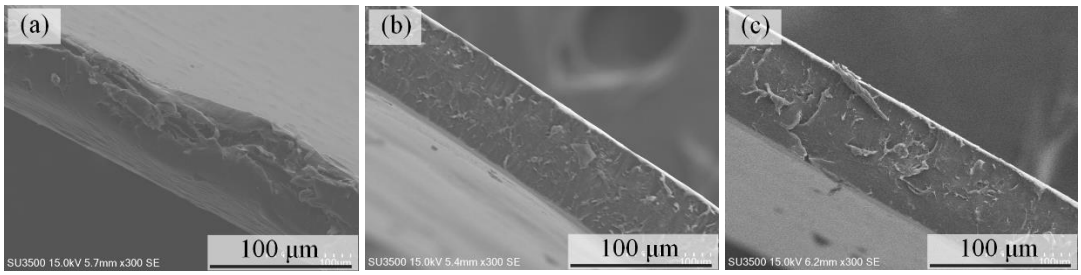

Figure 1-9. Cross section of (a) neat PLA, (b) PLA/CNF, and (c) PLA/CNFa composite films.

1.3.7 Mechanical Properties of PLA Composite Films

The tensile test was conducted to examine the improvement in mechanical strength of PLA composite films. Generally, the tensile strength of solution casting products will be lower compared with industrial blend methods for PLA.[18] As summarized in **Table 1-3**, the neat PLA film exhibited a tensile strength of 30.1 ± 3.0 MPa, whereas, after 1 wt% CNF was added in the film (PLA/CNF1), the average maximum tensile strength was slightly reduced to 29.0 ± 12.0 MPa due to the incompatibility of PLA and CNF. It is interesting to note that the standard deviation of the tensile strength of PLA/CNF composite film shows that some regions had high tensile strength, while the others were lower than the tensile strength of PLA. This observation confirms the inhomogeneity of PLA/CNF composite film. Moreover, the higher weight percentage of CNF (2 wt%) led to even lower tensile strength as low as 16.7 ± 2.4 MPa. This observation was mainly because of the fiber's high agglomeration and incompatibility with the PLA matrix. On the other hand, PLA/CNFa1 composite film with 1 wt% CNFA showed 37.6 ± 3.8 MPa (25% increment) due to better compatibility among the components. PLA/CNFa2 composite film exhibits a tensile strength of 20.9 ± 4.1 MPa, which was lower because of fiber agglomeration due to the high amount of fiber added to the PLA matrix. PLA composite films showed no significant difference in strain percentage for all films, which ranged from 2.0 to 4.4% elongation. To increase the elongation of PLA composites, generally, a plasticizer must be present within the films.[19] **Figure 1-10** revealed

that neat PLA film had a uniform breaking point on the surface. Cellulose fibers influenced PLA composite films as there is no breaking point developed before the break and CNF fibers were surfaced out because the films thinned during the tensile test. On the other hand, PLA/CNFa1 composite films showed small slits, whereas PLA/CNFa2 composite films possessed larger slits. These slits in PLA/CNFa can be because the CNFa fibers merged with the PLA matrix due to their high compatibility.

Table 1-3. Tensile strength and elongation of PLA composite films.

Composite films	Ave. max tensile str. (MPa)	Elongation (%)
Neat PLA	30.1 ± 3.0	2.0 ± 0.3
PLA/CNF1	29.0 ± 12.0	4.4 ± 1.9
PLA/CNF2	16.7 ± 2.4	2.2 ± 0.8
PLA/CNFa1	37.6 ± 3.8	3.1 ± 0.7
PLA/CNFa2	20.9 ± 4.1	2.5 ± 0.5

*Standard deviations were measured from the average of 8 specimens (each sample).

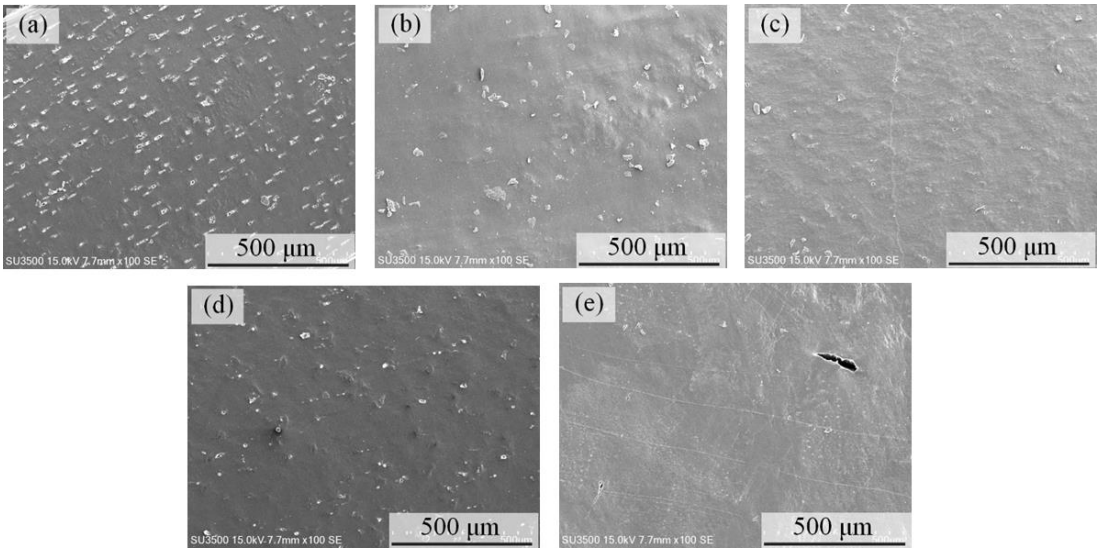

Figure 1-10. Break patterns of (a) neat PLA, (b) PLA/CNF1, (c) PLA/CNFa1, (d) PLA/CNF2, and (e) PLA/CNFa2 composite films after tensile test by using SEM.

1.3.8 Thermal Stability of PLA Composite Films

TGA was carried out to evaluate thermal stability, decomposition process, and kinetics of PLA composite films. As summarized in **Table 1-4** from TGA and DTG thermograms (**Figure 1-11** and **1-12**), there was no variation in the thermal degradation temperature, which ranged from 270.0 °C to 398.3 °C for neat PLA, PLA/CNF, and PLA/CNFa composite films. Maximum degradation temperatures were observed at 366.5 °C and 366.6 °C for PLA/CNF and PLA/CNFa composite films, respectively. This can be proved that additional CNF or CNFa maintained the thermal stability of PLA. Besides, the decomposition temperature of cellulose was ranging between 250 °C to 380 °C, and that can be the cause for the absence of double mass reduction due to the overlapping peaks.[20]

Table 1-4. Readings obtained from TGA thermogram.

Composite films	Decomposition temperature, T_d (°C)	Maximum decomposition temperature, T_{max} (°C)*
Neat PLA	289.1-397.8	366.0
PLA/CNF	270.0-394.7	366.5
PLA/CNFa	273.2-398.3	366.6

*From derivative thermogravimetric (DTG) curve obtained from TGA thermogram.

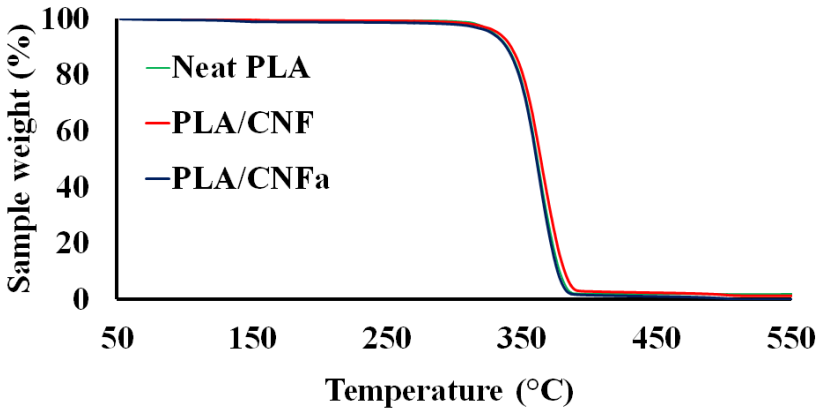

Figure 1-11 TGA thermograms of neat PLA composite films.

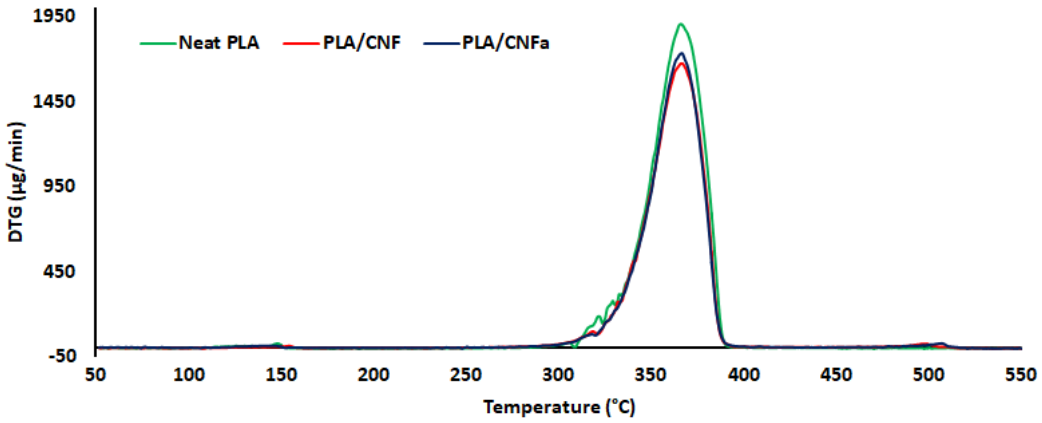

Figure 1-12 DTG thermogram of neat PLA, PLA/CNF, and PLA/CNFa composite films.

1.3.9 Degree of Crystallinity

The thermal properties of PLA composite films were investigated by DSC analysis as well. Based on the first heating of DSC thermograms, no significant variation was observed for the films. Meanwhile, PLA/CNF film showed the most amorphous structure as the degree of crystallinity obtained was 19.78%. **Table 1-5** summarized the compilations of crystallinity degree of PLA composite films (**Figure 1-13**). Although there is no significant variation in the degree of crystallinity among the films, there is some research indicated that slightly higher crystallinity (10% improvement) changed the transparency properties of PLA.[21]

Table 1-5. Degree of crystallinity for PLA composite films.

Composite films	Degree of crystallinity (%)
Neat PLA	23.64
PLA/CNF	19.78
PLA/CNFa	24.64

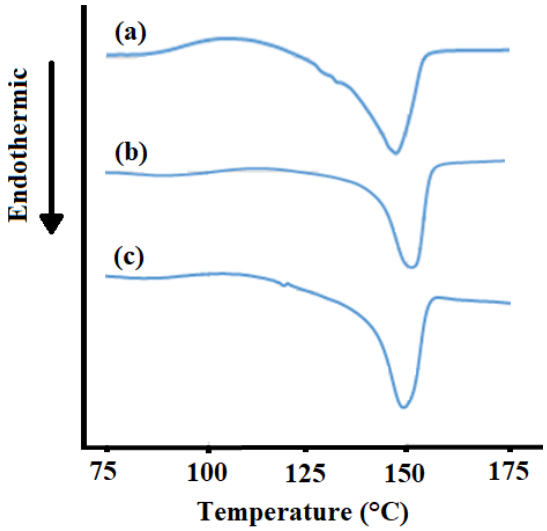

Figure 1-13. DSC thermograms of (a) neat PLA, (b) PLA/CNF, and (c) PLA/CNFa composite films for the first heating.

1.3.10 Hydrophobicity Behavior

Surface modification of cellulose changed the hydrophilicity of cellulose properties toward hydrophobic nature due to the substitution of the hydroxyl group into the acetyl group. Influences on the hydrophobicity of the samples were studied by static WCA measurement. Neat PLA showed an average contact angle of 70.2°, whereas those of PLA/CNF1 and PLA/CNFa1 were 71.3° and 75.9°, respectively. Higher wt% of fillers showed a much higher contact angle up to 80.4° and 85.9° for PLA/CNF2 and PLA/CNFa2, sequentially (**Table 1-6)**. PLA/CNFa composite films showed higher increments when compared with PLA/CNF for the same wt% of filler. The increment in hydrophobicity of the film surfaces can be due to the increased surface roughness of the films after the addition of fillers.[22]

Table 1-6. Contact angles measurement of PLA composite films.

Composite films	Water contact angles (degree)
Neat PLA	70.2 ± 1.1
PLA/CNF1	71.3 ± 2.7
PLA/CNF2	80.4 ± 3.7
PLA/CNFa1	75.9 ± 3.5
PLA/CNFa2	85.9 ± 2.1

*Standard deviations were measured from the average of 5 specimens (each sample).

1.4 Conclusions

This chapter demonstrated that CNF with a diameter of 69 ± 21 nm was prepared after five grind cycles and characterized. Then, CNF was acetylated into CNFa by the AA with DS values from 0.62 to 1.15 based on the reaction time and amount of AA used. The optimum reaction conditions in this research are 4 hours reaction time and 75 g of AA, which produced CNFa with DS 1.07. The compatibility of PLA films with cellulose fillers was enhanced and proved by SEM images on PLA/CNFA composite films as no obvious agglomeration was observed. CNFa (1 wt%) fillers improved the tensile strength of the films by 25% up to 37.6 ± 3.8 MPa, while neat PLA exhibited 30.1 ± 3.0 MPa. Furthermore, contact angles of PLA composite films were improved by 22.4% when CNFa (2 wt%) was added to the matrix indicated that the hydrophobicity of PLA/CNFa composite films enhanced after the addition of filler. PLA composites with CNFa with DS 1.07 possessed several advantages based on their preparation methods such as the efficient amount of product, higher compatibility, and better mechanical properties. Hence, the applications of PLA/CNFa composite films such as bio-based food packaging, can be enhanced and widen in the future.

1.5 References

1 M. Arrieta, M. Samper, M. Aldas and J. López, *Materials (Basel).*, 2017, **10**, 1008.

2 Y. Bor, J. Alin and M. Hakkarainen, *Packag. Technol. Sci.*, 2012, **25**, 427–433.

3 M. Murariu and P. Dubois, *Adv. Drug Deliv. Rev.*, 2016, 107, 17–46.

4 M. P. Arrieta and L. Peponi, *Eur. Polym. J.*, 2017, **89**, 174–184.

5 M. Johan Iskandar Zahari, N. Mohd Jahi, N. Hanisah Mohd, I. Ahmad, A. Baharum, A. Mat Lazim, S. Ramli and R. Othaman, , DOI:10.20944/preprints201807.0314.v1.

6 M. Jonoobi, A. P. Mathew, M. M. Abdi, M. D. Makinejad and K. Oksman, *J. Polym. Environ.*, 2012, **20**, 991–997.

7 A. Pei, Q. Zhou and L. A. Berglund, *Compos. Sci. Technol.*, 2010, **70**, 815–821.

8 T. Saito, S. Kimura, Y. Nishiyama and A. Isogai, *Biomacromolecules*, 2007, **8**, 2485–2491.

9 K. Y. Lee, J. J. Blaker and A. Bismarck, *Compos. Sci. Technol.*, 2009, **69**, 2724–2733.

10 J. H. Bae and S. H. Kim, *Polym. Int.*, 2015, **64**, 821–827.

11 P. Qu, Y. Zhou, X. Zhang, S. Yao and L. Zhang, *J. Appl. Polym. Sci.*, 2012, **125**, 3084–3091.

12 F. Quero, S. J. Eichhorn, M. Nogi, H. Yano, K. Y. Lee and A. Bismarck, *J. Polym. Environ.*, 2012, **20**, 916–925.

13 M. Bulota and M. Hughes, *J. Mater. Sci.*, 2012, **47**, 5517–5523.

14 P. Fei, L. Liao, B. Cheng and J. Song, *Anal. Methods*, 2017, **9**, 6194–6201.

15 E. W. Fischer, H. J. Sterzel and G. Wegner, *Kolloid-Zeitschrift Zeitschrift für Polym.*, 1973, **251**, 980–990.

16 I. Siró and D. Plackett, *Cellulose*, 2010, 17, 459–494.

17 N. Lin, J. Huang, P. R. Chang, J. Feng and J. Yu, *Carbohydr. Polym.*, 2011, **83**, 1834–1842.

18 J. R. Khurma, D. R. Rohindra and R. Devi, *South Pacific J. Nat. Appl. Sci.*, 2005, **23**, 22.

19 N. Ljungberg and B. Wesslén, *Biomacromolecules*, 2005, **6**, 1789–1796.

20 P. Rantuch and T. Chrebet, *THERMAL DECOMPOSITION OF CELLULOSE INSULATION*, 2014, vol. 48.

21 E. Kun and K. Marossy, *Mater. Sci. Forum*, 2013, **752**, 241–247.

22 A. C. C. De Leon, R. B. Pernites and R. C. Advincula, *ACS Appl. Mater. Interfaces*, 2012, **4**, 3169–3176.

Chapter 2

Effects of Acid Anhydrides-Modified Cellulose Nanofiber on Poly(lactic acid) Composite Films

2.1 Introduction

In each D-glucose unit of cellulose, there are three active hydroxyl groups. These groups can easily form hydrogen bonds, resulting in cellulose showing hydrophilicity. Cellulose is insoluble in common organic solvents and hydrophobic polymers.[1] After modification of the hydroxyl groups of cellulose, the hydrogen bonds are weakened and cellulose becomes more dispersible in organic solvents and most hydrophobic polymers.[2] Besides, cellulose is one of the best filler materials for polymer composites because of its high mechanical strength and biodegradability, and several functionalizations of cellulose have been studied and developed.[3] Various modifications of cellulose have been performed to improve the compatibility of cellulose with the polymer matrix.[4,5] Recently, our group successfully modified cellulose with citric acid to improve its compatibility with poly(propylene) and PLA resins.[6,7] Furthermore, the esterification of cellulose to produce hydrophobic products has been widely studied since the early 1980s.[8]

The dependence of the esterification effects of CNF on the starting reactants and their DSs is also an interesting topic. For example, Vice-Garcia et al.[9] investigated the dependence of the main transition of cellulose fatty esters on the length of their aliphatic substituents. In 2009, Crépy et al.[10] investigated the effect of saturated and unsaturated C12 to C18 chains on cellulose fatty esters and prepared polymer films from modified cellulose. Recently, the same group studied a series of fatty acid cellulose esters (FACEs) with various DS values and side-chain lengths from C10 to C16, and they compared the mechanical and chemical properties of each FACE.[11] A review of the various material functionalities based on thermoplastic cellulose and related structural

polysaccharide derivatives has been published.[12] In the review, they discussed the approaches for enabling effective thermoplasticization and incorporation of material functionalities, such as single-substituent derivatization, derivatization with multiple substituents, blending of simple derivatives, and graft copolymerization. The influences of short alkyl-chain substituents have also been investigated. For example, Yu et al.[13] modified cellulose with acid anhydrides to form modified cellulose with C1 to C3 alkyl-chain substituents, and then investigated their effects on the structure and thermal properties of cellulose-g-polyoxyethylene (2) hexadecyl ether. However, very limited research on the comparison of the effects of different alkyl-chain substituents of CNF on PLA composite films has been performed.

In this chapter, CNF was modified with AA, PA, and BA to form surface-modified CNFa, CNFp, and CNFb, respectively. The acylation method of the CNF was developed based on the method in chapter 1.[2] Fillers of m-CNFs with different DS values and lengths of the alkyl-chain substituents were used to fabricate PLA/m-CNF composite films with various transparency, strength, and wettability values. This work aims to investigate the effect of the acid anhydride on the rate of CNF acylation and the influence of the m-CNFs on the PLA composite films. The acylation reaction time was varied to obtain m-CNFs with various DS values and predict the rate of acylation. CNFa, CNFp, and CNFb differ in the length of the alkyl-chain substituents of the carbonyl groups (**Figure 2-1**), which varies from C1 to C3. The PLA/m-CNF composite films were expected to improve the mechanical and wettability properties. We focused on the dispersibility and optical, physical, and hydrophobic properties of the PLA/m-CNF composite films measured by UV–vis spectroscopy, a haze meter, SEM, tensile strength tests, and WCA measurements.

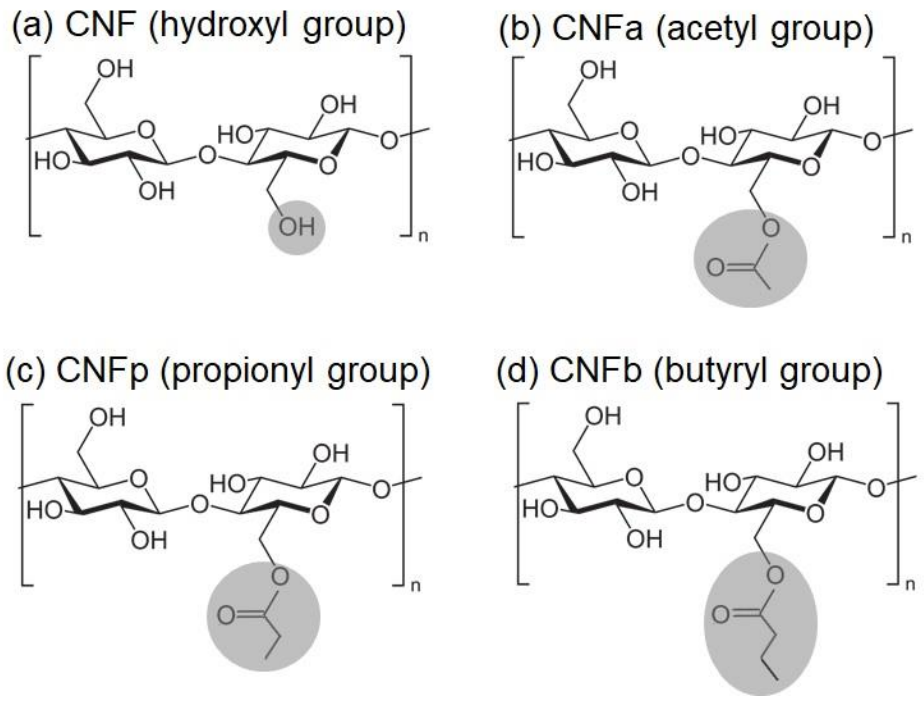

Figure 2-1. Chemical structures of (a) CNF, (b) CNFa, (c) CNFp, and (d) CNFb.

2.2 Experimental section

2.2.1 Materials

MCC was obtained from Merck Japan Ltd. (Tokyo, Japan). DMF was purchased from Kanto Chemical (Tokyo, Japan). AA, PA, BA, chloroform (>99.0%), and acetone (>99.0%) were obtained from Wako Pure Chemical Industries (Osaka, Japan) and used without further treatment. PLA (PLA2003D Ingeo biopolymer) was purchased from NatureWorks LLC (Minnesota, MN, USA). Water was treated with a Model III instrument from Organo Corporation (Tokyo, Japan) to produce deionized water (H_2O).

2.2.2 Preparation of CNF

CNF was prepared by following the method in chapter 1 without the study of its number of cycles. In this chapter, the cycle has proceeded to 10 cycles, and the suspension of CNF (1.57 wt%) in water was stored in a glass bottle and kept in a refrigerator (<4 °C).

2.2.3 Surface Modification of CNF

CNF modifications were developed from chapter 1 and in this chapter, several parameters were added. Other than AA, extra reactants of PA and BA also was used as the source of acid anhydrides. The acylation reaction time was varied from 1 to 4 h to investigate the reaction rate. The products of the m-CNFs are called CNFa*X* (AA modified), CNFp*X* (PA modified), and CNFb*X* (BA modified) based on their anhydride, where *X* is the reaction time (in h).

2.2.4 Preparation of PLA Composite Films

The solution casting method was used to prepare the PLA/m-CNF composites. First, a dispersion of unmodified CNF or m-CNF in chloroform (0.02 g of solid) was poured into a beaker, and chloroform was added to reach 50 g in total weight. Next, 2 g of PLA was added and the mixture was stirred for 3 h at room temperature. The mixture was then poured into a Petri dish and left overnight in a closed bio-shaker at 25 rpm and 40 °C to evaporate the chloroform. The samples are denoted neat PLA (without filler), PLA/CNF, PLA/CNFa, PLA/CNFp, and PLA/CNFb composite films.

2.2.5 Characterizations

An ATR-IR spectrometer (iD5 ATR, Thermo Scientific, Waltham, MA, USA) was used to determine the functional groups after modification. EDX spectroscopy was carried out to calculate the DS values of the produced m-CNFs using a Miniscope TM3000/SwiftED3000 system (Hitachi, Tokyo, Japan). For the DS calculation, C and O, but not H, were included. After acylation, the mass ratio of C is expected to increase relative to O owing to the increased C species from the acyl

groups that substitute for the H atoms of the hydroxyl groups of CNF. The transmittance and transparency values of the composite films were determined using a UV–vis spectrophotometer (U-2810, Hitachi, Tokyo, Japan) in the visible region (200–800 nm) scanned at a rate of 800 nm/min. The transparency values were calculated by **Equation 2-1**:

$$\textbf{Transparency} = \log \frac{\boldsymbol{T}\textbf{(average)}}{\boldsymbol{X}} \textbf{ (Equation 2-1)}$$

where $\boldsymbol{T}$**(average)** and $\boldsymbol{X}$ are the average UV–vis transmittance and average thickness of the film, respectively. A haze meter (NDH 4000, Nippon Denshoku) was used to calculate the haze values of the PLA/m-CNF composite films. The haze value was determined by **Equation 2-2**:

$$\textbf{Haze} = \frac{\textbf{T.T.} - \textbf{P.T.}}{\textbf{T.T.}} \times \textbf{100 (Equation 2-2)}$$

where **T.T.** and **P.T.** are the intensities of the transmitted light and parallel light, respectively. For the transmittance studies, two batches of PLA/m-CNF composite films with different thicknesses were fabricated. The thinner films were prepared by reducing the total amount of reactant to 1 g while maintaining their ratios. The morphologies of the PLA/m-CNF composite films were observed by SEM (SU3500, Hitachi, Tokyo, Japan) using Au–Pd sputter to increase the sample's surface conductivity. The samples were cut and attached to circular SEM plates (25 cm). For the surface morphology, magnification at 100× (500 μm scale) was used to provide a wide area of the film's surface. The mechanical properties of the composite films were investigated with a universal testing machine (EZ Graph, Shimadzu, Kyoto, Japan) following the JIS K6251-8 standard. Each sample was cut into dumbbell shapes for at least five tests and dried in an oven at 80 °C before analysis to remove any remaining solvent and moisture. The crosshead speed was 50 mm/min with a load cell of 100 N. The crystallinities of PLA/m-CNF composite films were calculated using DSC (EXSTAR 6000 DSC6220, SEIKO, Tokyo, Japan) from T_c and melting temperature T_m areas. The crystallinities of the PLA composite films were calculated using the theoretical $\Delta \boldsymbol{H_f}$ (93.1 J g^{-1}).[14]

$$\Delta Hm - \Delta Hc = \Delta H' \text{ (Equation 2-3)}$$

$$\frac{\Delta H'}{\Delta Hf} \text{ x } 100 = X_c \text{ \% (Equation 2-4)}$$

$$\Delta H_f = 93.1 \text{ J/g}$$

where, ΔH_m and ΔH_c are the enthalpies given during melting and crystallization, respectively, and X_c % is the degree of crystallinity. The wettability of the films was investigated by WCA measurement using a Drop Master DM300 contact angle meter (Kyowa Interface Science, Tokyo, Japan) with FAMAS basic software. Each sample was dried in an oven at 80 °C before analysis. The WCAs were measured for at least seven specimens.

2.3 Results and Discussion

2.3.1 Surface Modifications of CNF

ATR-IR was performed to observe the acyl groups that substituted the hydroxyl groups of CNF after modification. The ATR-IR spectra of the m-CNFs are shown in **Figure 2-2**. New peaks appeared at around 1730 cm^{-1}, corresponding to the C=O stretching vibration modes of the carbonyl group between CNF and the anhydrides. This indicates that the acyl groups from the anhydrides were incorporated into the CNF to become CNFa, CNFp, and CNFb. Moreover, the increases in the intensities of the carbonyl peaks with increasing reaction time showed that the acylation processes were proportional to the reaction time. The intensities of the –OH deformation of water peaks at around 1650 cm^{-1} were higher than the intensities of the C=O stretching peaks for all of the m-CNFs after 1-h acylation. This changed when the acylation time was increased to 2 h, where the intensities of the carbonyl peaks were higher than those of the –OH deformation of water peaks. Furthermore, the intensities of the C=O stretching peaks were higher for 4-h acylation compared with both 1- and 2-h acylation, indicating that the DS for 4-h acylation was the highest among the studied reaction times.

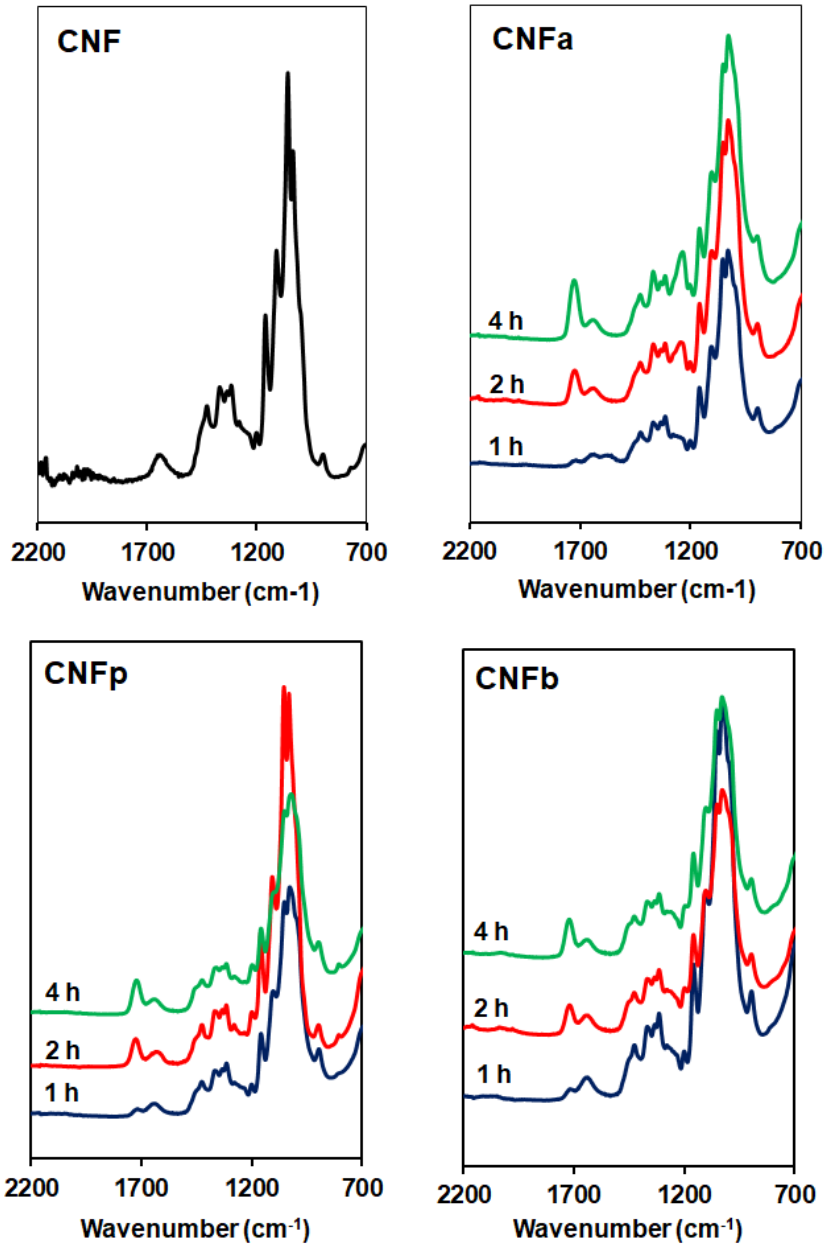

Figure 2-2. ATR-IR spectra of CNF, CNFa, CNFp, and CNFb.

2.3.2 DS of m-CNFs

EDX spectroscopy has a probe depth of 1–3 μm, while the average diameter of the CNF was about 63 ± 17 nm. The average diameter was calculated based on the SEM image in **Figure 2-3**. EDX indicates the composition of each element, and therefore the DS values of the CNF and m-CNFs can be calculated. The modification percentages of the m-CNFs with respect to the reaction time are shown in **Figure 2-4**. The modification percentages increased with increasing reaction time from 1 to 4 h. The rates of acylation of CNFa and CNFp were almost the same and exponentially increased with the reaction time, while CNFp showed a slightly higher acylation rate. However, the acylation rate of CNFb showed that the acylation rate was significantly lower for a longer alkyl-chain substituent. Longer alkyl-chain of the anhydride (BA) leads to a slower rate reaction due to steric effect and lower surface area compared to AA and PA.[15] After the 1 h reaction, only 9.8% of CNFb was modified, which was the lowest among the m-CNFs. For 4 h reaction time, 24.5% of CNFb was modified, while 29.4% and 31.4% of CNFa and CNFp were modified, respectively. The EDX results further verified that the acyl groups were chemically bonded to the CNF and acylation increased with increasing reaction time. The DS values of the m-CNFs were calculated from the percentage modified values using **Equation 2-5** to **2-8**:

CNF = $C_6H_{10}O_5$ (M_w = 162 g/mol); mass percentages (excluding H): C = 47.3%, O = 52.7%

The theoretical ratio of C:O $= \frac{C}{O} = \frac{47.3}{52.7} = 0.897$

Assuming that 100% CNF is modified to CNFa,

CNFa = $C_{12}H_{16}O_8$ (M_w = 288 g/mol)

Mass percentages (excluding H): C = 52.9%, O = 47.1%

$$\boldsymbol{A}\% = \textbf{percentage of CNF acetylate } (\textbf{CNFa})$$

$$\boldsymbol{B} = \textbf{ratio of C:O} = \frac{\textbf{C}}{\textbf{O}}$$

$$\boldsymbol{B = \frac{C}{O} = \frac{Mw \text{ of single C } [\text{No of C acetylate } (A\%) + \text{No of C in CNF } (100\% - A\%)]}{Mw \text{ of single O } [\text{No of O acetylate } (A\%) + \text{No of O in CNF } (100\% - A\%)]}}$$

$$\boldsymbol{B = \frac{C}{O} = \frac{12[12(A\%) + 6(100\% - A\%)]}{16[8(A\%) + 5(100\% - A\%)]}}$$

Simplify A%:

$$\boldsymbol{A\% = \frac{900 - 1000B}{6B - 9}}$$ **(Equation 2-5)**

Assuming that 100% CNF is modified to CNFp,

CNFp = $C_{15}H_{22}O_8$ (M_w = 330 g/mol); mass percentages (excluding H): C = 58.4%, O = 41.6%

$P\% =$ percentage of CNF propionate (CNFp)

$$\boldsymbol{B = \text{ratio of C:O} = \frac{C}{O}}$$

$$\boldsymbol{B = \frac{C}{O} = \frac{Mw \text{ of single C } [\text{No of C propionate } (P\%) + \text{No of C in CNF } (100\% - P\%)]}{Mw \text{ of single O } [\text{No of O propionate } (P\%) + \text{No of O in CNF } (100\% - P\%)]}}$$

$$\boldsymbol{B = \frac{C}{O} = \frac{12[15(P\%) + 6(100\% - P\%)]}{16[8(P\%) + 5(100\% - P\%)]}}$$

Simplify P%:

$$\boldsymbol{P\% = \frac{200\ (10B - 9)}{3\ (9 - 4B)}}$$ **(Equation 2-6)**

Assuming that 100% CNF is modified to CNFb,

CNFb = $C_{18}H_{28}O_8$ (M_w = 372 g/mol); mass percentages (excluding H): C = 62.8%, O = 37.2%

$\boldsymbol{B\% = \text{percentage of CNF butyrate (CNFb)}}$

$$\boldsymbol{B = \text{ratio of C:O} = \frac{C}{O}}$$

$$\boldsymbol{B = \frac{C}{O} = \frac{Mw \text{ of single C } [\text{No of C butyrate } (B\%) + \text{No of C in CNF } (100\% - B\%)]}{Mw \text{ of single O } [\text{No of O butyrate } (B\%) + \text{No of O in CNF } (100\% - B\%)]}}$$

$$\boldsymbol{B = \frac{C}{O} = \frac{12[18(B\%) + 6(100\% - B\%)]}{16[8(B\%) + 5(100\% - B\%)]}}$$

Simplify B%:

$$\boldsymbol{B\% = \frac{450 - 500B}{3\ (B - 3)}}$$ **(Equation 2-7)**

$$\textbf{Degree of substitution (DS)} = \frac{\textbf{percentage modified}}{\textbf{100\%}} \times \textbf{3 (Equation 2-8)}$$

From the EDX instrument, the value of *B* can be obtained, which is the C:O mass ratio. Therefore, the DS of m-CNF can be calculated from the derived equations and the results are given in **Table 2-1**. EDX for each sample was measured four times and averaged to calculate the DS.

Table 2-1. DS values of the m-CNFs based on the reaction time.

Reaction time (hours)	Degree of substitution (DS)		
	CNFa	CNFp	CNFb
1	0.41	0.45	0.29
2	0.75	0.81	0.47
4	0.88	0.94	0.74

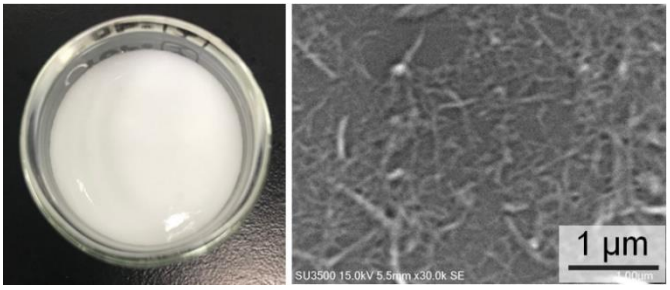

Figure 2-3. Suspension of CNF in water and its SEM image at ×30,000 magnification.

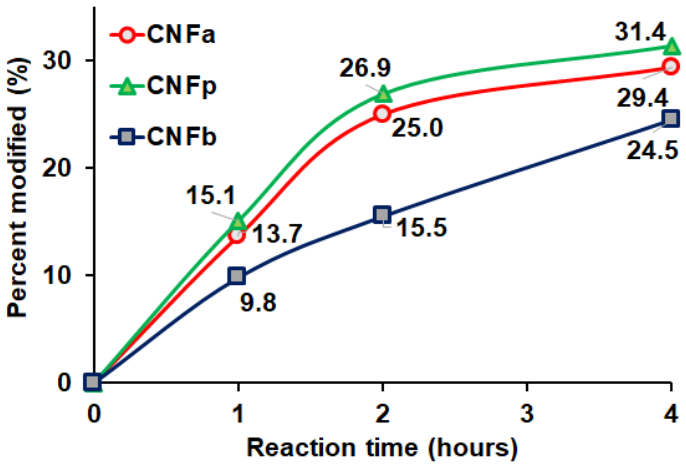

Figure 2-4. Percentage of m-CNF with respect to the reaction time for CNFa, CNFp, and CNFb.

2.3.3 Optical Transmittances of PLA Composite Films

Photographs of the PLA/m-CNF composite films are shown in **Figure 2-5**. The patterns in the background can be observed through the neat PLA film, demonstrating that the film possessed very good transparency (**Figure 2-5a**). The white agglomerates observed on the PLA/CNF composite film (**Figure 2-5b**) are because of their inhomogeneity with the PLA matrix. CNF tends to form agglomerates in the matrix because of their opposite hydrophilicity. Agglomerates of CNFa2, CNFp2, CNFa4, and CNFp4 in the PLA matrix were confirmed to be minimal because the background can still be observed without any precipitation of the fillers. Even though the PLA/CNFb4 composite film (**Figure 2-5h**) exhibited high transparency because the background can be observed, the lower DS of CNFb2 (PLA/CNFb2 composite film) (**Figure 2-5g**) resulted in poor visibility of the background. This might be because the lower DS of CNFb2 (0.47) makes the unmodified CNF (in CNFb2) have a more significant effect on the PLA/m-CNF composite film, and hence reduces its miscibility with the PLA matrix. In addition, the surfaces of the films with the CNFb filler were rougher than those with the CNFa and CNFp fillers regardless of their DS. As previously mentioned, the m-CNFs (DS > 0.47) have high compatibility with PLA because of

their similar hydrophobicity. For this reason, the PLA/CNFa, PLA/CNFp, and PLA/CNFb4 composite films showed better transparency than the PLA/CNF and PLA/CNFb2 composite films.

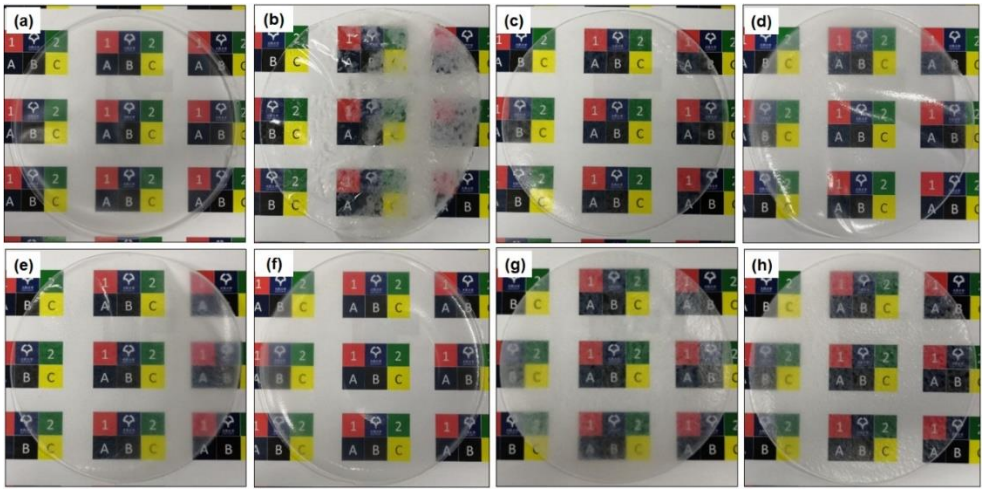

Figure 2-5. Photographs of the (a) neat PLA, (b) PLA/CNF, (c) PLA/CNFa2, (d) PLA/CNFa4, (e) PLA/CNFp2, (f) PLA/CNFp4, (g) PLA/CNFb2, and (h) PLA/CNFb4 composite films.

2.3.4 Light Transmittances of PLA Composite Films

UV–vis spectroscopy was performed to compare the transparency of the PLA/m-CNF composite films by calculating the percentage of UV–vis transmittance. We compared two batches of PLA/m-CNF composite films with different thicknesses. The different thickness films were prepared by using different initial amounts of reactant (1 and 2 g) during the preparation of the films. The average transmittance values (**Table 2-2**) were used as relative values for comparison. Thicker films show lower transparency because the amount of light that passes through the films is reduced. All of the films prepared with a larger amount of reactant showed UV–vis transmittance below 42.2%, including the neat PLA film. Furthermore, the additional filler decreases the transparency because the light is scattered/diffracted by the filler regardless of the thickness. Even though there was a very large difference between the UV–vis transmittance of the thick and thin

films, both batches of PLA/m-CNF composite films showed the same pattern with respect to the filler. For 1 g of the reactant, the neat PLA film showed 89.3% transmittance, which was the highest among all of the films. The heterogeneous nature of the PLA/CNF composite film decreased the transmittance to 77.8%. This is lower than that of the PLA film because of the formation of agglomerates, which result in diffraction and scattering of light during UV–vis analysis. Also, PLA with the CNFb2 filler (DS = 0.47) showed lower transmittance (77.9%) than the neat PLA film (89.3%) owing to the low compatibility between the filler and PLA. The composite films of PLA with the other m-CNF fillers showed better transmittance (81.0%–83.9%). This can be attributed to the better and more uniform dispersion of the relatively high DS (≥0.74) m-CNFs in the PLA matrix compared with unmodified CNF or low DS m-CNFs. The transmittance spectra of the PLA/m-CNF composite films (1 g) in the visible wavelength region (400–800 nm) are shown in **Figure 2-6**, which were used to calculate the transparency values of the films. The transparency values were calculated based on the specific thickness of each film. All of the transparency values followed the same pattern as the UV–vis transmittance regardless of the amount of reactant used.

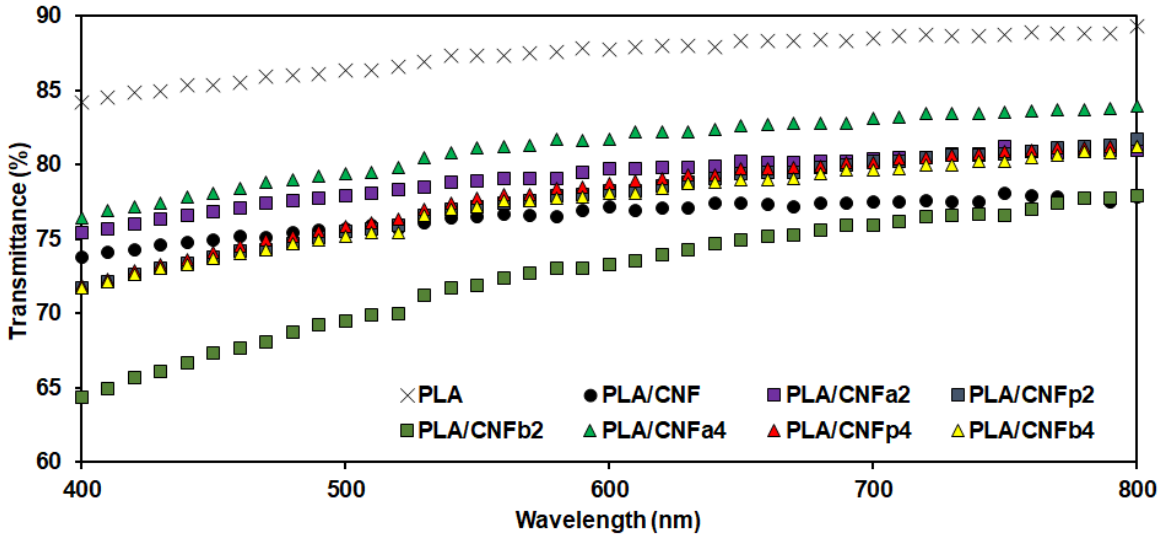

Figure 2-6. UV–vis transmittance of the PLA/m-CNF composite films (1 g of reactant).

Table 2-2. Average thickness, transmittance, and transparency values of the PLA/m-CNF composite films.

Films	DS of fillers	Thicknesses (μm)		UV-Vis transmittance (%)		Transparency values	
		1 g	2 g	1 g	2 g	1 g	2 g
Neat PLA	-	51	190	89.3	39.1	3.23	2.31
PLA/CNF	-	82	231	77.8	13.2	2.97	1.76
PLA/CNFa2	0.75	65	238	81.0	26.8	3.08	2.05
PLA/CNFp2	0.81	64	213	81.7	25.8	3.08	2.08
PLA/CNFb2	0.47	81	232	77.9	25.3	2.95	2.04
PLA/CNFa4	0.88	60	224	83.9	34.9	3.13	2.19
PLA/CNFp4	0.94	57	177	81.2	42.2	3.14	2.38
PLA/CNFb4	0.74	52	256	81.2	22.3	3.18	1.94

2.3.5 Haze Transmittances of PLA Composite Films

To further support the UV–vis transmittance, the haze values of the films were determined (**Table 2-3**). The haze values increased with the addition of the fillers for both amounts of the reactants. For 1 g of the reactant, the neat PLA film gave the lowest haze value of 6.8%. The poor dispersions of CNF and CNFb2 showed haze values of 35.5% and 30.0%, respectively. Adding the m-CNF fillers changed the haze values to between 17.5% and 19.5% (except for CNFb2), which can be considered to be good for transparent films. The increase of the haze value from that of the neat PLA is because the fillers increased the amount of reflected and scattered light. The

compatibility and dispersion of the higher DS m-CNF fillers in the PLA matrix are the key factors for achieving lower haze values compared with the PLA/CNF and PLA/CNFb2 composite films. For 2 g of the reactant, the haze transmittance was not reliable because the neat PLA film exhibited a higher haze value than the PLA/CNFp2, PLA/CNFa4, and PLA/CNFp4 composites. Also, the remaining haze values of the PLA/m-CNF composite films showed inconsistency when compared with the 1 g films. For example, the PLA film with the CNFb4 filler showed a high haze value for the 2 g film (81.7%) which was significantly different from those of the other films with m-CNF fillers. In contrast, the film with 1 g of the same filler exhibited a haze value of 19.0%, which was close to the haze values of the other m-CNF fillers.

Table 2-3. Average thicknesses and haze values of the PLA/m-CNF composite films.

Films	DS of fillers	Thicknesses (μm)		Haze values (%)	
		1 g	2 g	1 g	2 g
Neat PLA	-	51	190	6.8	48.8
PLA/CNF	-	82	231	35.5	93.0
PLA/CNFa2	0.75	65	238	19.5	50.0
PLA/CNFp2	0.81	64	213	17.8	40.2
PLA/CNFb2	0.47	81	232	30.0	76.7
PLA/CNFa4	0.88	60	224	20.1	41.9
PLA/CNFp4	0.94	57	177	17.5	28.0
PLA/CNFb4	0.74	52	256	19.0	81.7

2.3.6 Morphologies of PLA Composite Films

The CNF filler resulted in different physical properties of the PLA matrix in comparison with the m-CNFs fillers, especially on the surface, because of the difference in their compatibility. The PLA film (**Figure 2-7a**) showed a smooth surface because there was no filler involved. The PLA/CNF composite film had a rough surface (**Figure 2-7b**), and it was clear that the CNF filler caused agglomeration on/in the PLA matrix. Hence, the PLA/CNF composite film showed a lumpy surface with clear white agglomerates. In contrast, the PLA/m-CNF composite films with CNFa4 and CNFp4 as fillers (**Figure 2-7d** and **2-7f**) exhibited flat and smooth surfaces because of their good compatibility with the PLA matrix. These results demonstrate that acylation changed the compatibility of the CNF with the PLA matrix for CNFa and CNFp. The relatively high DS m-CNF fillers were expected to have high compatibility with PLA owing to their hydrophobicity, while the hydrophilic CNF and relatively low DS m-CNFs were expected to have low compatibility with PLA. The SEM images showed that the scattered fillers on the surface were related to the DS of the m-CNF fillers. As the DS of the m-CNF decreased, the filler became more observable, as shown in **Figures 2-7c** and **2-7e**. This indicates that the compatibility between the PLA matrix and m-CNF filler is affected by the difference in the DS values. As discussed in the earlier section, the surfaces of the PLA/CNFb composite films were both rough. The SEM images of the PLA/CNFb composite films (**Figure 2-7g** and **2-7h**) are in agreement with those observations because the PLA/CNFb composite films were rough. The DS of CNFb4 is 0.74, which is almost the same as that of CNFa2 (DS = 0.75), so the difference in the lengths of the alkyl-chain substituents might be the cause of this opposite observation. It seems that the butyryl group substituted on the hydroxyl group of CNF tends to shield and localize CNFb, and hence rough surfaces are observed for the PLA/CNFb composite films regardless of their DS. Morphology differences of the m-CNFs are observed in the SEM images (**Figure 2-8**). After modification with acid anhydrides, the structures

of the m-CNFs changed and higher DS m-CNFs produced smaller agglomerates. CNFb4 (DS = 0.74) formed relatively large agglomerates, which might lead to a rougher surface during PLA/CNFb composite film preparation. It appears that the higher number of the hydroxyl groups in CNFb4 (due to lower DS than CNFa4 and CNFp4) formed opposite interaction between unmodified and modified parts of CNFb4, hence, larger agglomerates were formed during dispersion in chloroform.

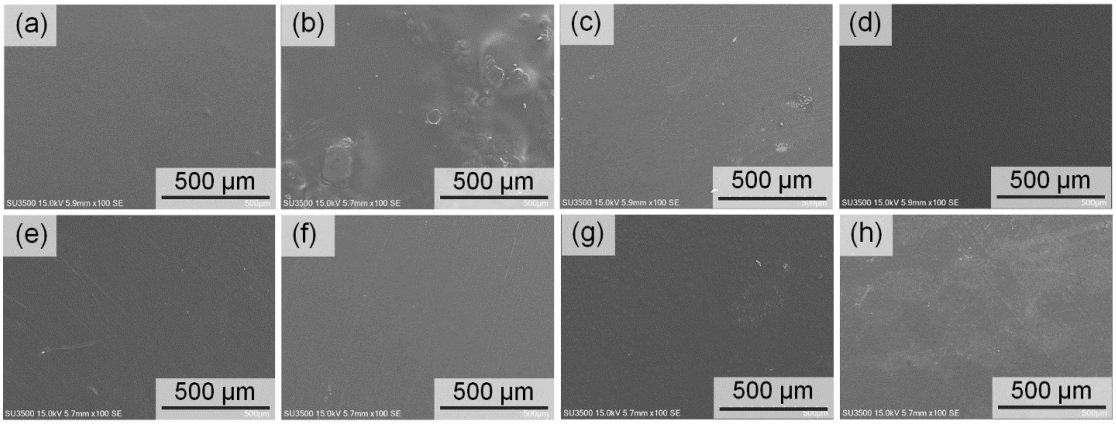

Figure 2-7. SEM images of the (a) neat PLA, (b) PLA/CNF, (c) PLA/CNFa2, (d) PLA/CNFa4, (e) PLA/CNFp2, (f) PLA/CNFp4, (g) PLA/CNFb2, and (h) PLA/CNFb4 composite films.

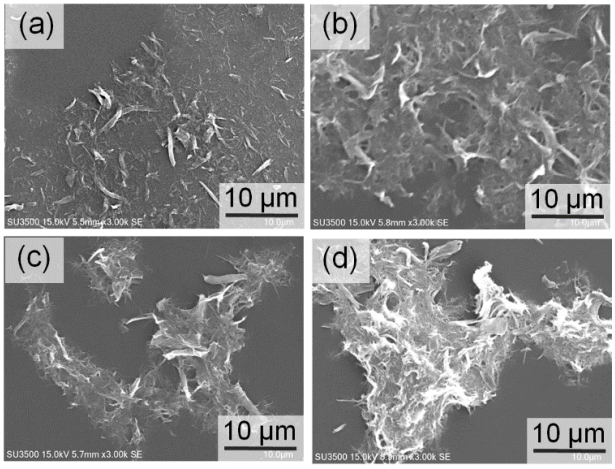

Figure 2-8. SEM images of (a) CNF, (b) CNFa4 (DS = 0.88), (c) CNFp4 (DS = 0.94), and (d) CNFb4 (DS = 0.74) at ×3000 magnification.

Other than surface morphologies, the cross-section of the films was also observed (**Figure 2-9**). It is interesting to note that neat PLA and PLA/CNF composite films display plastic-like deformation after cracked (**Figure 2-9(a-b)).** It was proven that CNF is not compatible with the PLA matrix. Meanwhile, **Figures 2-9(c-h)** show that the m-CNFs are incorporated with the PLA matrix by forming stack-like morphologies.

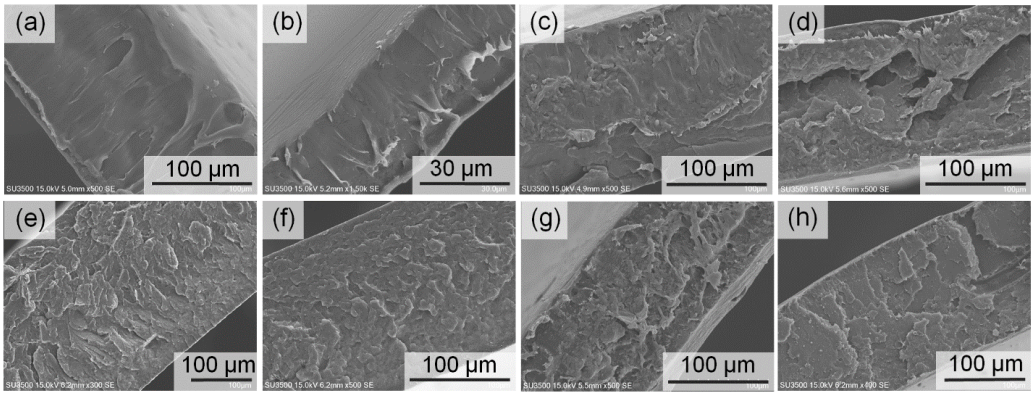

Figure 2-9. Cross-section images of the (a) neat PLA, (b) PLA/CNF, (c) PLA/CNFa2, (d) PLA/CNFa4, (e) PLA/CNFp2, (f) PLA/CNFp4, (g) PLA/CNFb2, and (h) PLA/CNFb4 composite films.

2.3.7 Mechanical Properties of PLA Composite Films

The mechanical properties of the films are given in **Table 2-4**. The neat PLA film showed a tensile strength of 46.1 ± 4.5 MPa, and the inclusion of CNF in the PLA matrix decreased the tensile strength (23.9 ± 5.8 MPa). The decrease in the tensile strength of the PLA/CNF composite film was because of the inhomogeneity between the PLA matrix and CNF filler. The DS of the m-CNF played an important role in determining the tensile strength of the PLA/m-CNF composite film. Regardless of the filler species, all of the films with fillers of DS < 0.76 (CNFa2, CNFb2, and CNFb4) exhibited lower tensile strength than the neat PLA film. Conversely, the fillers with DS > 0.80 showed higher tensile strength, with the PLA/CNFp4 composite film showing the highest

tensile strength of 53.0 ± 2.4 MPa. Both the CNFa4 (DS = 0.88) and CNFp2 (DS = 0.81) fillers also improved the tensile strength of the PLA/m-CNF composite films compared with the neat PLA film. Therefore, the tensile strength of the PLA film can be improved by the addition of m-CNF with DS > 0.80. In general, composites prepared by the solution casting method have lower tensile strength than those prepared by the melt blend method.[16] This occurred for products in this study as well because the tensile strength for the PLA in this research was lower than that of pure commercialized or industrial PLA. The neat PLA film showed Young's modulus of 1.24 ± 0.28 GPa. The differences among Young's modulus values of the PLA/m-CNF composite films showed the same pattern as the tensile strength, except for the CNFa fillers. Even though the PLA matrix with the CNFa2 filler showed lower tensile strength than the neat PLA film (by 11%), it's Young's modulus was about 14% higher. In contrast, the PLA/CNFa4 composite showed higher tensile strength than the neat PLA film, but it's Young's modulus was lower (1.07 ± 0.10 GPa). Regarding the strain to failure, there were no significant differences among the strain percentages of the PLA/m-CNF composite films (2.4%–3.9% with standard deviations of 0.1–1.4). The areas under the strain–stress curves (**Figure 2-10**) were calculated to predict the tensile toughness values of the films. Although the PLA/m-CNF composite films showed good tensile strength and modulus, their toughness was relatively poor, the same as general PLA.[17]

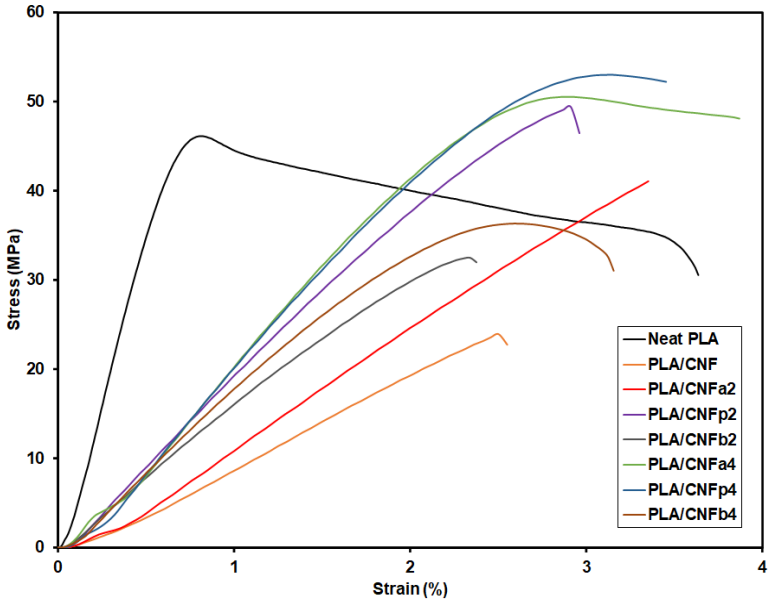

Figure 2-10. Stress-strain curves of PLA/m-CNF composite films.

Table 2-4. Mechanical properties of the PLA/m-CNF composite films.

Composite films	Tensile stress (MPa)	Young's modulus (GPa)	Tensile strain (%)	Toughness (J/mm^3)
Neat PLA	46.1 ± 4.5	1.24 ± 0.28	3.6 ± 0.5	1.54 ± 0.21
PLA/CNF	23.9 ± 5.8	1.00 ± 0.39	2.5 ± 0.4	0.25 ± 0.08
PLA/CNFa2	41.1 ± 0.2	1.41 ± 0.57	3.3 ± 1.4	0.49 ± 0.03
PLA/CNFp2	49.4 ± 3.0	1.75 ± 0.08	3.0 ± 0.4	0.80 ± 0.14
PLA/CNFb2	32.5 ± 1.4	1.23 ± 0.17	2.4 ± 0.3	0.90 ± 0.59
PLA/CNFa4	50.5 ± 2.1	1.07 ± 0.10	3.9 ± 0.5	1.65 ± 0.01
PLA/CNFp4	53.0 ± 2.4	1.74 ± 0.09	3.5 ± 0.1	1.31 ± 0.21
PLA/CNFb4	36.3 ± 0.1	1.08 ± 0.21	3.2 ± 0.2	0.81 ± 0.18

*Standard deviations were measured from the average of 5 specimens (each sample).

2.3.8 Crystallinity of the PLA Composite Films

Both transparency and mechanical properties of PLA can be affected by the crystallinity of the samples.[18] Calculated from DSC thermograms (**Figure 2-11**), the X_c of PLA/m-CNF composite films is obtained and reported in **Table 2-5**. X_c of PLA/m-CNF composite films was lower compared to neat PLA (39.6%) due to the formation of aggregates, which decreased the number of nucleating sites [19]. PLA/m-CNF composite films showed that no significant variation was observed regardless of the m-CNFs' substituent groups, which varies from 30.7% to 33.1%. Meanwhile, PLA/CNF composite film showed the most amorphous structure at X_c of 16.2% due to the incompatibility between CNF filler and PLA matrix, hence, forming more aggregates than m-CNFs fillers. Therefore, PLA/CNF composite films exhibited a lower amount of nucleating sites.

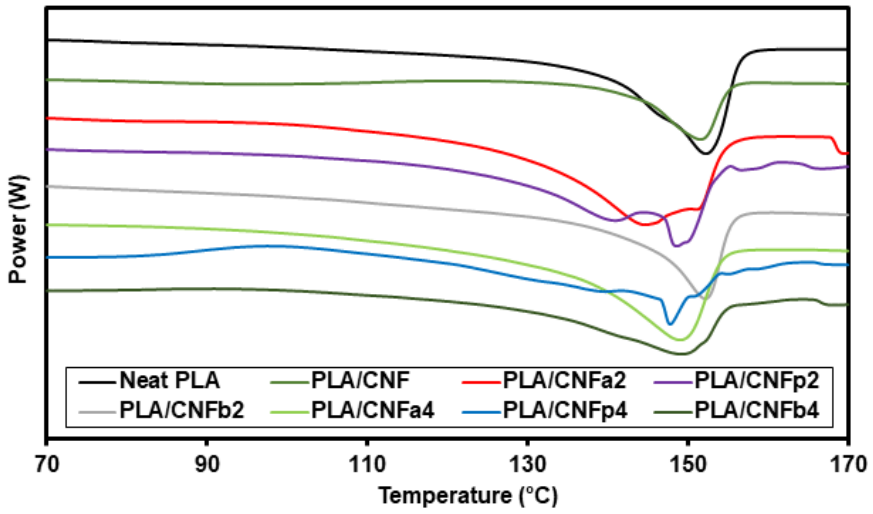

Figure 2-11. DSC thermograms of PLA/m-CNF composite films.

Table 2-5. The degree of crystallinity for PLA/m-CNF composite films.

Films	Degree of crystallinity, X_c (%)
Neat PLA	39.6
PLA/CNF	16.2
PLA/CNFa2	32.4
PLA/CNFp2	28.2
PLA/CNFb2	28.1
PLA/CNFa4	30.7
PLA/CNFp4	33.1
PLA/CNFb4	28.6

2.3.9 Wettability of PLA Composite Films

The WCAs of the neat PLA and PLA/m-CNF composite films are shown in **Figure 2-12**. The neat PLA film showed an average WCA of 83.9°, whereas that of the PLA/CNF composite film was 81.7°. This shows that the PLA/CNF filler had higher wettability owing to the hydrophilicity of CNF. All of the PLA/m-CNF composite films showed higher WCAs than the neat PLA and PLA/CNF films regardless of the filler and DS. This is attributed to a change from hydrophilic CNF to hydrophobic CNFa, CNFp, and CNFb. Substitution of the acyl groups for the hydroxyl groups of CNF is the main reason for the hydrophobicity. From the discussion in Section 3.1, the number of hydrogen bonds of CNF decreases when the hydroxyl groups are substituted by hydrophobic acyl groups. Therefore, the wettability of the PLA film decreases by adding m-CNF fillers compared with unmodified CNF. Based on the results in **Figure 2-12**, the length of the alkyl-chain substituent had a significant effect on the wettability of the PLA/m-CNF composite film. Comparing the fillers with the same acylation time, PLA/CNFb showed the highest WCA values for both reaction times (87.3° and 88.5° for the CNFb2 and CNFb4 fillers, respectively). This indicates that the substituted propionyl group of CNFb increased the hydrophobicity of the PLA/m-CNF composite film even though the DS was lower than those of both CNFa and CNFp. Also, a comparison between CNFa and CNFp showed that the CNFa fillers had lower hydrophobicity (WCAs of 85.3° and 86.0° for CNFa2 and CNFa4, respectively) owing to their shorter alkyl-chain substituents.

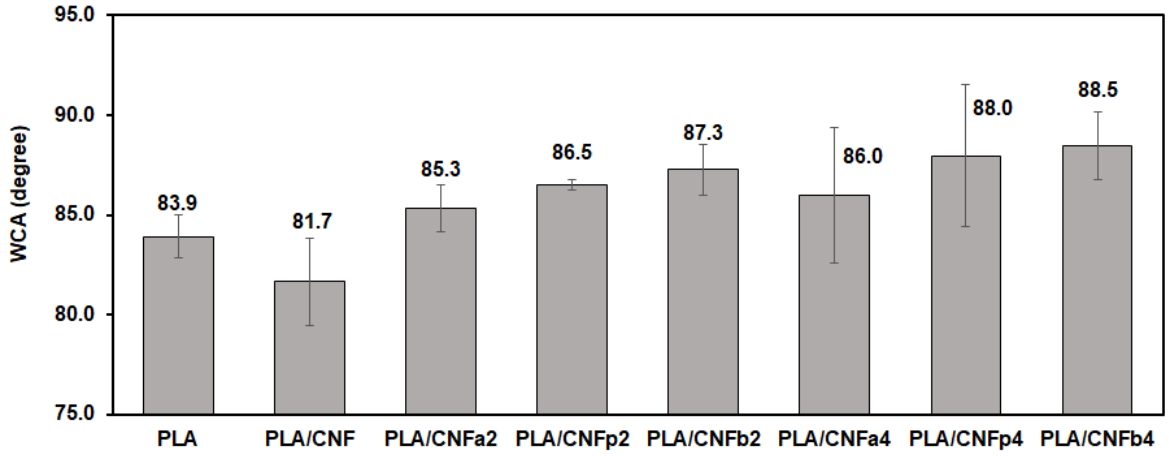

Figure 2-12. Wettability of the PLA composite films. Standard deviations were measured from the average of 8 specimens (each sample).

2.4 Conclusion

In this study, CNF was acylated using acid anhydrides with short alkyl-chain substituents (C1 to C3), followed by the fabrication of PLA/m-CNF composite films. CNFp showed the highest rate of acylation among the m-CNFs, and reaction for 4 h produced 31.4% CNFp, which was the highest among all of the studied parameters. The introduction of CNF as a filler decreased the transparency, mechanical, and wettability properties compared with the neat PLA film. Conversely, the compatibility of the m-CNFs with the PLA matrix was mostly improved. By comparison of the films, the effects of different m-CNFs on PLA were investigated. The PLA/CNFp4 composite films showed the best transparency and mechanical properties, which was mainly because CNFp4 had the highest DS. Therefore, the DS of the filler is the key factor to improve the properties of PLA/m-CNF composite films. Meanwhile, the low DS CNFb2 filler (DS = 0.47) showed inhomogeneity of the matrix–filler interaction because the unmodified CNF part of CNFb2 had a more significant effect on the composite. Thus, the transparency and mechanical properties of the PLA/CNFb2 composite film were lower than those of the other PLA/m-CNF films. However, according to the WCA, the wettability of the PLA/CNFb2 composite film improved. Based on these observations, it was concluded that a longer alkyl-chain substituent (CNFb filler) had a greater influence than the DS of the filler on the wettability properties of the PLA/m-CNF composite films.

2.5 References

1 Y. Zhang, H. Li, X. Li, M. E. Gibril, K. Han and M. Yu, *J. Polym. Res.*, 2013, **20**, 1–9.

2 N. Jamaluddin, T. Kanno, T. A. Asoh and H. Uyama, *Mater. Today Commun.*, 2019, **21**, 100587.

3 A. Shalwan and B. F. Yousif, *Mater. Des.*, 2013, **48**, 14–24.

4 A. Pei, Q. Zhou and L. A. Berglund, *Compos. Sci. Technol.*, 2010, **70**, 815–821.

5 T. Saito, S. Kimura, Y. Nishiyama and A. Isogai, *Biomacromolecules*, 2007, **8**, 2485–2491.

6 X. Cui, T. Honda, T. A. Asoh and H. Uyama, *Carbohydr. Polym.*, 2020, **230**, 115662.

7 X. Cui, A. Ozaki, T. A. Asoh and H. Uyama, *Polym. Degrad. Stab.*, 2020, **175**, 109118.

8 J. Dixon, P. Andrews and L. G. Butler, *Biotechnol. Bioeng.*, 1979, **21**, 2113–2123.

9 C. Vaca-Garcia, G. Gozzelino, W. G. Glasser and M. E. Borredon, *J. Polym. Sci. Part B Polym. Phys.*, 2003, **41**, 281–288.

10 L. Crépy, L. Chaveriat, J. Banoub, P. Martin and N. Joly, *ChemSusChem*, 2009, **2**, 165–170.

11 L. Duchatel-Crépy, N. Joly, P. Martin, A. Marin, J. F. Tahon, J. M. Lefebvre and V. Gaucher, *Carbohydr. Polym.*, 2020, **234**, 115912.

12 Y. Teramoto, *Molecules*, 2015, 20, 5487–5527.

13 W. Yu, N. Han, Y. Qian, X. Zhang and W. Li, *Polymers (Basel).*, 2018, **10**, 498.

14 E. W. Fischer, H. J. Sterzel and G. Wegner, *Kolloid-Zeitschrift Zeitschrift für Polym.*, 1973, **251**, 980–990.

15 D. L. F. DeTar, *J. Org. Chem.*, 1980, **45**, 5174–5176.

16 J. R. Khurma, D. R. Rohindra and R. Devi, *South Pacific J. Nat. Appl. Sci.*, 2005, **23**, 22.

17 S. Farah, D. G. Anderson and R. Langer, *Adv. Drug Deliv. Rev.*, 2016, 107, 367–392.

18 E. Kun and K. Marossy, *Mater. Sci. Forum*, 2013, **752**, 241–247.

19 M. Perić, R. Putz and C. Paulik, *Eur. Polym. J.*, 2019, **114**, 426–433.

Chapter 3

Acylation of Cellulose nanofiber as Filler for Poly(methyl methacrylate) Composite Films Reinforcement

3.1 Introduction

In recent decades, various transparent polymers such as PMMA, PS, and PC have gained attention because of their excellent optical clarity. As one of the transparent polymers, PMMA is an important material with good processability that has been used for several applications such as windows, lenses, and optical devices. Also, PMMA is often used as a substitute for glass material because of its high mechanical-dynamical properties and optical transparency. However, the applications of PMMA are limited owing to its insufficient mechanical strength and impact resistance, which limit its efficiency in engineering applications.[1] Therefore, some research has been conducted to overcome these limitations by preparing composites of PMMA via reinforcement with nano- and micro-sized fibers.[2–4] Cellulose is a great candidate as a filler to counter the drawbacks of PMMA due to its high mechanical strength and biodegradability.[5]

Many attempts have been made to prepare PMMA composites with various types of cellulose. For instance, Kiziltas et al. prepared PMMA/cellulose composites by varying the type of cellulose and studied their effect on the properties of the composites.[6] They managed to slightly improve the physical properties of PMMA; however, its transparency was significantly reduced even with the addition of a low amount of fillers. In 2017, Anju and Narayanankutty tried to improve the adhesion of PMMA and MCC by adding bis-(3-triethoxysilylpropyl) tetrasulfide as a coupling agent.[7] Due to chemically bonded PMMA and MCC, the physical properties were greatly improved; however, they did not mention the optical properties of the product.

Acylation is another example of CNF modification that can alter its hydrophilicity and prevent the wetting behavior of CNF. Hence, it is expected to improve compatibility with PMMA matrices. In the past year, research on thermoplasticization and acylation of several types of cellulose has been widely conducted by numerous methods, mainly for improving its water repellency without any specific applications.[8–10] However, very limited research has been reported on using acylated CNF as a reinforcement material in a PMMA matrix.

In this chapter, PMMA composites reinforced with surface acylated CNF are presented. The objective of this work is to evaluate the dispersion improvement of CNF in a PMMA matrix while maintaining its high transparency by surface-modified CNF. Here, CNFa and CNFp were prepared and their dispersibility in PMMA was evaluated. The PMMA and acylated CNF composites were also expected to improve transparency, mechanical strength, and wettability. Comparing CNF, CNFa, and CNFp, aggregation was observed in CNF, whereas the dispersibility of CNFa and CNFp in PMMA was improved by surface modification. Furthermore, in the comparison between CNFa and CNFp, the hydrophobicity composites were improved by using CNFp with a long alkyl chain length.

3.2 Experimental section

3.2.1 Materials

MCC was obtained from MERCK Japan Ltd. (Tokyo, Japan). DMF was purchased from Kanto Chemical (Tokyo, Japan). PA, AA, chloroform >99.0%, and acetone >99.0% were obtained from Wako Pure Chemical Industries (Osaka, Japan) and used without treatment. PMMA (Mw = 125,000) was purchased from Sigma Aldrich (St. Louis, MO, USA). Water was treated using a model III instrument from Organo Corporation (Tokyo, Japan) to produce deionized water (DI-H_2O).

3.2.2 Preparation and Modification of CNF

CNF was prepared by following the method in chapter 1 without the study of its number of cycles. In this chapter, the cycle has proceeded to 5 cycles, and the suspension of CNF (1.57 wt%) in water was stored in a glass bottle and kept in a refrigerator (<4 °C). Meanwhile, CNF modifications were developed from chapter 2 and in this chapter, only AA and PA were used as the source of acid anhydrides. BA was exempted because of its low efficiency as filler in chapter 2.

3.2.3 Preparation of PMMA Composite Films

The solution casting method was used to prepare PMMA composites. First, a dispersion of CNF, CNFa, or CNFp in chloroform (0.02 g or 0.04 g of solid content for 1 wt% or 2 wt%, respectively) was poured into a beaker, and chloroform was added to reach 50 g in total weight. Next, 2 g of PMMA were added and the mixture was stirred for 1 h at room temperature. The mixture was then poured into a petri dish and left overnight in a closed bio-shaker at 25 rpm and 40 °C to evaporate the chloroform. The samples were denoted as neat PMMA (without filler), PMMA/CNF, PMMA/CNFp, and PMMA/CNFa composite films. Throughout this study, CNFp and CNFa with a 4 h reaction time were used as fillers. The main processes involved in this research are illustrated in **Figure 3-1**.

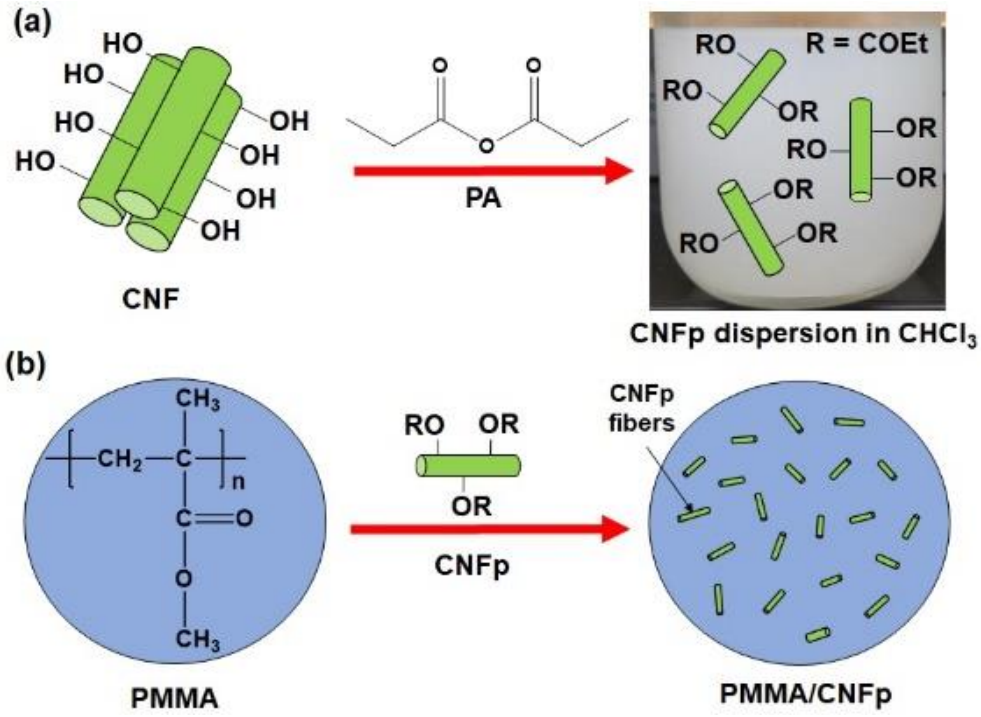

Figure 3-1. Schematic illustrations of (a) acylation process by using PA and (b) PMMA/CNFp composite film preparation.

3.2.4 Characterizations

An ATR-IR instrument (iD5 ATR, Thermo Scientific, Waltham, MA, USA) was used to observe functional groups after modification. Electron-dispersive X-ray (EDX) spectroscopy was carried out to calculate the DS of CNFp produced using a Miniscope TM3000/SwiftED3000, Hitachi, Tokyo, Japan. For the DS calculation in this research, C and O elements, but not H, were included. After acylation, the mass ratio of C was expected to increase relative to O due to increased C species from the propionyl groups that substitute for H in hydroxyl groups of CNF (**Figure 3-2**). **Equations 3-1** to **3-2** were derived and further used for the calculations:

Assume 100% glucose units of CNF are modified into CNFp,

CNFp = $C_{15}H_{22}O_8$ (Mw = 330 $gmol^{-1}$); mass percentage (excluding H), C = 58.4%, O = 41.6%

$$\boldsymbol{A = Percent\ of\ CNF\ propionate\ (CNFp); B = Ratio\ of\ C{:}O = \frac{C}{O}}$$

$$\boldsymbol{B = \frac{C}{O} = \frac{Mw\ of\ single\ C\ [No\ of\ C\ propionate\ (A) + No\ of\ C\ in\ CNF\ (100\% - A)}{Mw\ of\ single\ O\ [No\ of\ O\ propionate\ (A) + No\ of\ O\ in\ CNF\ (100\% - A)}}$$

$$\boldsymbol{B = \frac{C}{O} = \frac{12[15(A) + 6(100\% - A)}{16[8(A) + 5(100\% - A)}}$$

Simplify A,

$$\boldsymbol{A = \frac{200\ (10B - 9)}{3\ (9 - 4B)}}$$ **(Equation 3-1)**

$$\boldsymbol{DS = \frac{A}{100} \times 3}$$ **(Equation 3-2)**

where $\boldsymbol{A}$ is the percentage of acylation (%) and $\boldsymbol{B}$ is the mass ratio of C to O (C:O) for CNFp.

The morphology of the PMMA composite films was observed with an SEM instrument (SU3500, Hitachi, Tokyo, Japan) using Au–Pd sputter to increase the sample's surface conductivity. Samples were cut and attached to circular SEM plates (25 cm). For surface morphology, magnification at 100× (500 μm scale) was used to provide a wide area of the film's surface. The transmittance of the composite films was determined using a UV-vis spectrophotometer (U-2810 spectrophotometer, Hitachi, Tokyo, Japan) in the visible region (200–800 nm) scanned at a rate of 800 nm/min. A haze meter (NDH 4000, Nippon Denshoku) was employed to calculate the haze values of the PMMA composite films. The haze value was measured using **Equation 3-3**:

$$\mathbf{Haze} = \frac{\mathbf{T.T.} - \mathbf{P.T.}}{\mathbf{T.T.}} \times \mathbf{100}$$ **(Equation 3-3)**

where **T.T.** and **P.T.** are the intensities of the whole transmitted light and parallel light, respectively. The mechanical properties of the composite films were investigated using a universal testing machine (EZ Graph, Shimadzu, Kyoto, Japan) following the JIS K6251-8 standard. Each sample was cut into dumbbell shapes for at least 5 tests and dried in an oven at 80 °C before analysis to remove any remaining solvent and moisture. The crosshead speed was 50 mm/min with a load cell of 100 N. Also, tensile toughness was measured by calculating the area under stress-strain curves.

The wettability of the films was studied with a WCA test using a Drop Master DM300, Kyowa Interface Science, Tokyo, Japan, with FAMAS basic software. Each sample was dried in an oven at 80 °C before analysis, measured for at least 6 specimens.

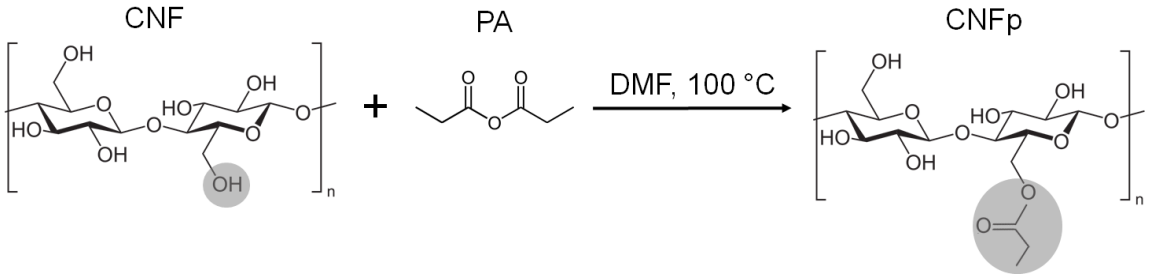

Figure 3-2. The chemical equation of the acylation process of CNF into CNFp.

3.3 Results and discussion

3.3.1 Surface Modifications of CNF

ATR-IR was used to observe the substitution of acyl/acetyl groups at the hydroxyl groups of CNF after modification. **Figure 3-3** shows a new peak appearing around 1730 cm^{-1} after acylation by IR measurement, corresponding to the C=O stretching vibration modes of the carbonyl group between CNF and PA. This indicates that the propionyl group from PA is incorporated into the CNF to become CNFp. Moreover, the change in intensity of the carbonyl peaks based on different reaction times provides some insight into the kinetics of the acylation process. A longer reaction time produces a higher carbonyl peak intensity, which demonstrates that the acylation process increases with reaction time.

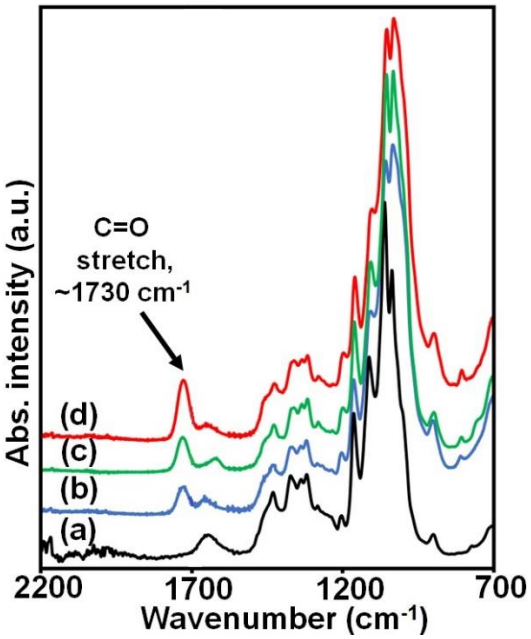

Figure 3-3. ATR-IR spectra of (a) CNF, (b) CNFp (1 h), (c) CNFp (2 h), and (d) CNFp (4 h).

3.3.2 DS of m-CNFs

EDX spectroscopy has a probed depth of 1–3 μm, while the average diameter of CNF in this study was about 69 ± 21 nm.[11] EDX indicates the composition of each element and therefore the DS of CNF and m-CNFs can be calculated. Based on this, the ratios of C and O of the CNF were 47.3% and 52.7%, respectively. As shown in **Table 3-1**, the CNF mass ratio in this study was very close to the theoretical value. Therefore, the results are significant for use in this study. After acylation, the ratio of C increased with an increase in reaction time. The results showed that 51.8% acylation occurred with a DS of 1.55 after 4 h of reaction time. There was approximately a 21.1% increase in acylation compared to that after 2 h of reaction time. As expected, the 1 h reaction time had a lower DS (0.62), with only 20.8 % of acylation occurring. The EDX results further confirm that the propionyl group was chemically bonded on CNF and that the acylation increased with reaction time. EDX for each sample was measured four times and averaged to calculate the DS.

Table 3-1. DS of CNFp based on reaction time.

Species	Mass concentration (%)		Ratio	Modify %
	C	O	(C:O)	(DS)
CNF	47.7	52.3	0.91	0 (0)
CNFa	49.7	50.3	0.99	29.4 (0.88)*
CNFp (1 hour)	51.2	48.8	1.05	20.8 (0.62)
CNFp (2 hours)	52.5	47.5	1.11	30.7 (0.92)
CNFp (4 hours)	55.0	45.0	1.22	51.8 (1.55)

*DS of CNFa is calculated by using different equations due to its different molecular weights.

3.3.3 Morphologies of PMMA Composite Films

CNF fillers resulted in different physical properties for the PMMA matrix in comparison with CNFa and CNFp fillers, especially on the surface, because of differences in their compatibility. As shown in **Figure 3-4a**, the PMMA/CNF composite film has a rough surface, and it is clear that CNF fillers cause agglomeration on/in the PMMA matrix. Hence, the PMMA/CNF composite film shows a lumpy surface with clear white agglomerations. In contrast, the PMMA/CNFa composite film (**Figure 3-4b**) exhibits a flat and smooth surface, similar to that found in the PMMA/CNFp composite films with 1 wt% (**Figure 3-4c**) and 2 wt% (**Figure 3-4d**) CNFp. CNFa and CNFp were expected to have higher compatibility with PMMA owing to their hydrophobicity, while the hydrophilic CNF was expected to have less compatibility with PMMA. The SEM images show that the CNFp filler is scattered on the surface but barely observed in the PMMA/CNFp1 composite film. This indicates that the compatibility between the PMMA matrix and CNFp filler is improved. The 2 wt% CNFp is more observable, mainly due to its higher concentration, which led to the

agglomeration of the filler. Likewise, the CNFa filler scattered on the PMMA matrix is difficult to see in the PMMA/CNFa composite film. These results demonstrate that acetylation and acylation can change the compatibility of CNFs with a PMMA matrix. Thus, the agglomeration of CNFs can be avoided by using CNFa or CNFp instead of unmodified CNF.

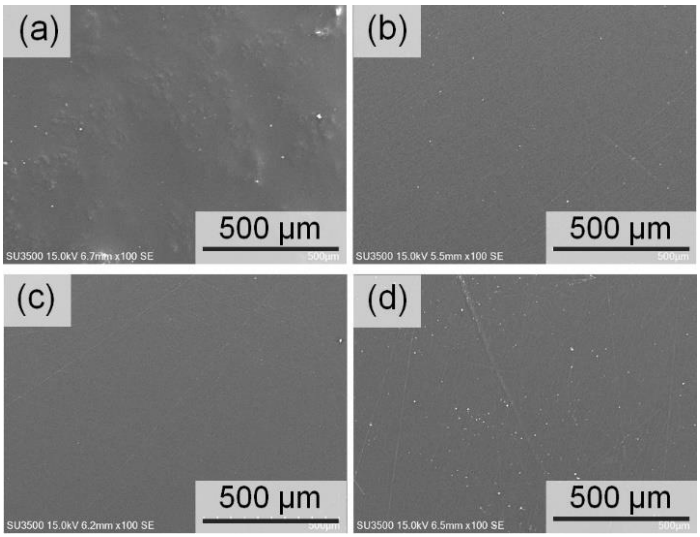

Figure 3-4. SEM images of (a) PMMA/CNF, (b) PMMA/CNFa, (c) PMMA/CNFp1, and (d) PMMA/CNFp2 composite films.

3.3.4 Optical Transmittance of PMMA Composite Films

Figure 3-5 shows photographs of PMMA composite films with different concentrations and types of fillers. The patterns in the background can be observed clearly through the films, demonstrating that all films maintain the transparency of PMMA. However, the black-colored background clearly shows the white agglomeration of CNF fillers on the PMMA/CNF composite film (**Figure 3-5b**). Agglomeration of CNFa and CNFp in the matrix was confirmed to be minimal as the black background can still be observed clearly without any precipitation of fillers. Some white agglomerations observed on PMMA/CNFp2 composite film (**Figure 3-5e**) are due to its high

concentration of CNFp filler. As previously mentioned, CNFa and CNFp have high compatibility with PMMA because of their similar hydrophobicity. For this reason, the PMMA/CNFa and PMMA/CNFp composite films have better transparency compared to the PMMA/CNF composite film.

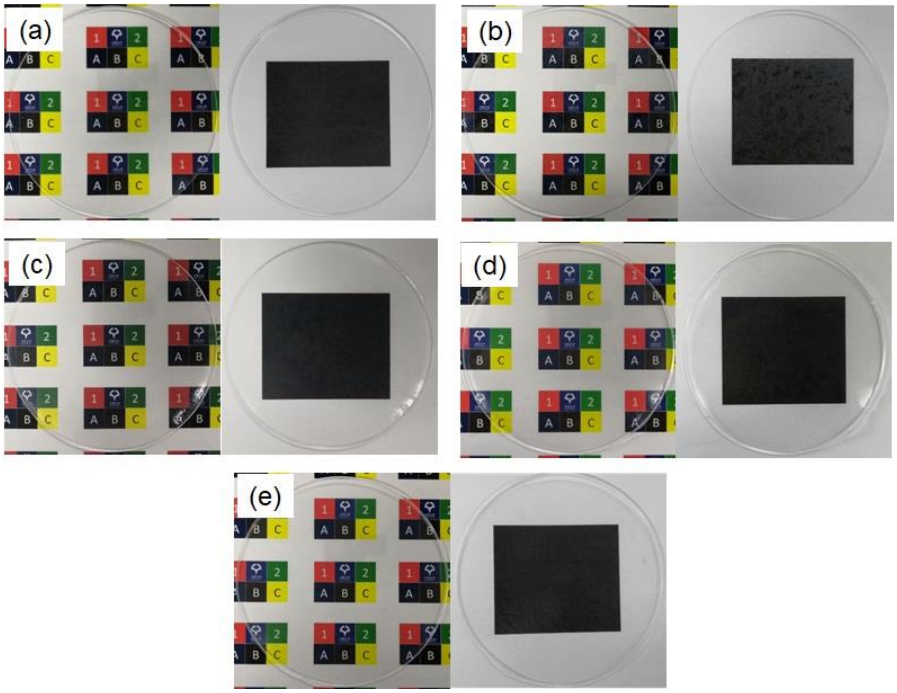

Figure 3-5. Photographs of (a) neat PMMA, (b) PMMA/CNF, (c) PMMA/CNFa, (d) PMMA/CNFp1, and (e) PMMA/CNFp2 composite films.

3.3.5 Light Transmittance of PMMA Composite Films

UV-vis spectroscopy was carried out to compare transparency among PMMA composite films by calculating the percentage of UV-vis transmittance. Transmittance spectra of PMMA composite films in the visible wavelength region (400–800 nm) are shown in **Figure 3-6**. The average transmittances, summarized in **Table 3-2**, were used as relative values for comparison. The neat PMMA film shows 79.6% transmittance, which is the highest among all the PMMA

composite films. The heterogeneous nature of the PMMA/CNF composites reduces its transmittance to 66.2%, lower because of agglomeration, which results in diffraction and scattering of light during UV-vis analysis. Composite films of PMMA with m-CNFs fillers have better transmittances, of 73.5% (CNFa), 71.6% (1 wt% CNFp), and 69.9% (2 wt% CNFp). These results can be attributed to the better and uniform dispersion of m-CNFs in the PMMA matrix instead of unmodified CNF.

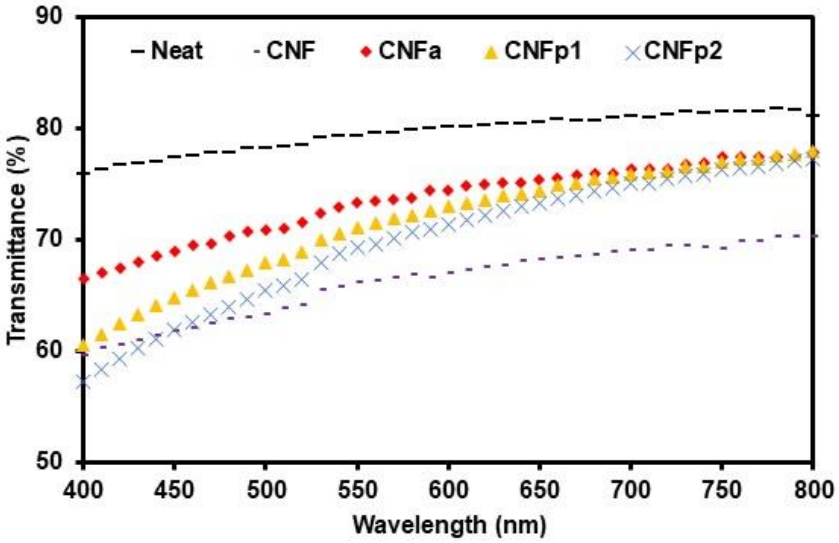

Figure 3-6. UV-vis transmittance of PMMA composite films.

Table 3-2. Haze values, average thickness, and transmittances of PMMA composite films.

Composite films	**T.T.** (%)	**P.T.** (%)	Haze values (%)	Average thickness (μm)	Average transmittance (%)
Neat PMMA	91.9	83.7	8.4	235	79.6
PMMA/CNF	88.5	66.0	25.5	194	66.2
PMMA/CNFa	90.2	76.2	15.5	189	73.5
PMMA/CNFp1	90.2	75.2	16.7	206	71.6
PMMA/CNFp2	90.3	75.7	16.1	203	69.9

3.3.6 Haze Transmittance of PMMA Composite Films

Table 3-2 summarizes the haze values, including T.T. and P.T. of the PMMA composite films. Neat PMMA gave the lowest haze value among the films at 8.39%. After the addition of CNF fillers, the haze value rises to 25.5%. This is because the CNF fibers agglomerate during the composite film preparation, increasing the amount of reflected and scattered light. In comparison with the PMMA/CNF composite film, the haze values of the PMMA/CNFp composite films significantly decrease to 16.7% and 16.1% for 1 wt% and 2 wt% of CNFp, respectively. Compatibility and dispersion of the CNFp filler in the PMMA matrix are the key factors for achieving a lower haze value compared to the PMMA/CNF composite films. The PMMA/CNFa composite film shows a slightly lower haze value of 15.5% due to its better transparency. The film thickness was calculated to confirm its effect on the optical properties of the films. The results in **Table 3-2** clearly show that thickness had no significant impact on the UV-vis transmittances or haze values.

3.3.7 Mechanical Properties of PMMA Composite Films

Table 3-3 shows mechanical property values for the films. The neat PMMA film exhibits a tensile strength of 33.1 ± 0.5 MPa, and CNF in the PMMA matrix does not cause any increase in tensile strength. The PMMA/CNF composite film's tensile strength is 31.3 ± 10.5 MPa owing to the incompatibility of PMMA and CNF, also suggested by the large standard deviation value. Certain regions in the film had lower tensile strength than neat PMMA, while other areas had higher values, confirming the inhomogeneity of CNF in the PMMA matrix. In contrast, CNFa and CNFp in the PMMA matrix show an increase of approximately 20–28% compared to the neat PMMA because of better compatibility between the components. Tensile strength values for PMMA/CNFa, PMMA/CNFp1, and PMMA/CNFp2 are 40.0 ± 7.7, 41.2 ± 2.9, and 42.3 ± 5.9 MPa, respectively. It is interesting to note that the tensile strength is increased by a slight when CNFp2 is added

compared to PMMA/CNFp1. This is because the higher concentration of CNFp leads to inhomogeneity of filler with the PMMA matrix. Therefore, the increment recorded in PMMA/CNFp2 is lower by the less uniformity of the matrix and filler. Generally, the product of solution casting possesses lower tensile strength compared to the melt blend method, which explains why the tensile strength of PMMA in this research is lower than that of pure commercialized or industrial PMMA.[12] The neat PMMA exhibits Young's modulus of 0.89 ± 0.13 GPa. Based on the same reason as tensile strength, the addition of CNF filler slightly reduces the modulus to 0.85 ± 0.09 GPa, while CNFa and CNFp fillers enhance the modulus to 1.04 ± 0.03 and 1.26 ± 0.07 GPa, respectively. As for the strain to failure, the PMMA composite films show no significant difference in strain percentage for all films, which ranges from 3.5% to 4.4% with a standard deviation of 0.2 to 1.0. **Figure 3-7** shows stress-strain curves for tensile toughness calculations. Furthermore, the toughness of neat PMMA film seems to increase by 78% when CNFa was added as filler. PMMA/CNFp1 and PMMA/CNFp2 composite films recorded an increment of 62% and 121%, respectively. It was proven that the compatibility of m-CNFs with the PMMA matrix leads to the increment of PMMA's toughness. On the other hand, the PMMA matrix with unmodified CNF filler has no significant improvement in toughness.

Table 3-3. Average tensile strength, Young's modulus, average elongation, and toughness of PMMA composite films.

Composite films	Tensile stress (MPa)	Young's modulus (GPa)	Tensile strain (%)	Toughness ($x10^3$ kJ/mm^3)
Neat PMMA	33.1 ± 0.5	0.89 ± 0.13	3.8 ± 0.6	0.63 ± 0.01
PMMA/CNF	31.3 ± 10.5	0.85 ± 0.09	3.8 ± 1.0	0.65 ± 0.44
PMMA/CNFa	40.0 ± 7.7	1.04 ± 0.03	4.1 ± 0.8	1.12 ± 0.35
PMMA/CNFp1	41.2 ± 2.9	1.26 ± 0.07	3.5 ± 0.2	1.02 ± 0.06
PMMA/CNFp2	42.3 ± 5.9	1.08 ± 0.13	4.4 ± 0.9	1.39 ± 0.46

*Standard deviations were measured from the average of 5 specimens (each sample).

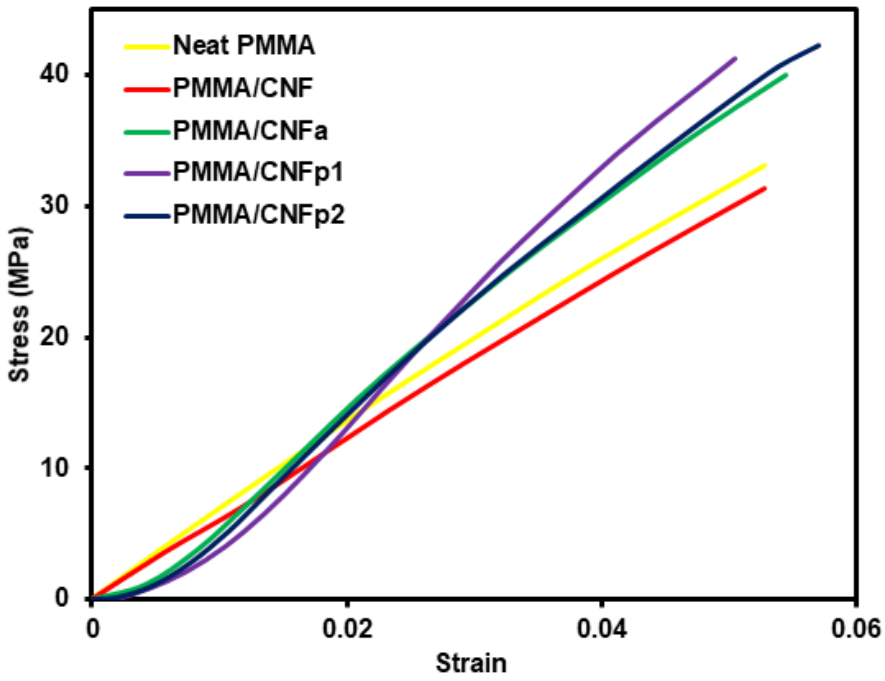

Figure 3-7. Stress-strain curve from the tensile test of PMMA composite films.

3.3.8 Wettability of PMMA Composite Films

As summarized in **Table 3-4**, neat PMMA shows an average WCA of 83.0°, whereas those of the PMMA/CNF composite film are 81.2°. It was demonstrated that CNF fillers have higher wettability due to CNF hydrophilicity. On the other hand, the CNFa and CNFp fillers have higher WCAs of 84.1°, 85.3°, and 86.2° for PMMA/CNFa, PMMA/CNFp1, and PMMA/CNFp2 composite films, respectively. These observations are attributed to a change from hydrophilic CNF to hydrophobic CNFa and CNFp. The substitution of acetyl and propionyl groups at the hydroxyl groups of CNF is the main reason for this hydrophobicity. Hydrogen bonding of CNF is reduced and hydroxyl groups are substituted by hydrophobic acetyl and propionyl groups. Therefore, the wettability of PMMA composite films can be reduced by introducing hydrophobized CNF instead of unmodified CNF fillers. CNFp filler provided slightly higher hydrophobicity than CNFa because the alkyl chain is slightly longer in the propionyl group of CNFp than in the acetyl group of CNFa, which slightly improves the hydrophobicity.

Table 3-4. Wettability of PMMA composite films.

Composite films	Water contact angle (degree)
Neat PMMA	83.0 ± 0.7
PMMA/CNF	81.2 ± 0.9
PMMA/CNFa	84.1 ± 3.4
PMMA/CNFp1	85.3 ± 0.4
PMMA/CNFp2	86.2 ± 1.0

*Standard deviations were measured from the average of 6 specimens (each sample).

3.4 Conclusions

In this chapter, CNF was successfully modified into CNFp by substituting the hydroxyl group of CNF for a propionyl group from PA. By increasing the reaction time to 4 h, the DS of CNFp was improved to a value of 1.55 (51.8% acylation). PMMA composite films with CNF, CNFp, and CNFa as fillers were successfully fabricated by the solution casting technique. Comparison of transparency between composites with fillers showed that CNFp and CNFa have better compatibility with the PMMA matrix. The results obtained from images, UV-vis transmittance, and haze values confirmed that the PMMA matrix transparency was maintained. In comparison with neat PMMA and PMMA/CNF composite films, the mechanical properties of PMMA/CNFa and PMMA/CNFp were enhanced. Uniform dispersion of the CNFp and CNFa in the PMMA matrix is a key factor for this enhancement. Furthermore, the wettability of the PMMA composite films was reduced by the introduction of CNFp, resulting in a higher WCA for the PMMA/CNFp composite films. In general, the influence of CNFp and CNFa as fillers on the PMMA matrix was not very different and the transparency of the PMMA/CNFp composite films was slightly lower. Meanwhile, its mechanical and wettability properties were slightly enhanced compared to those of the PMMA/CNFa composite film. In conclusion, the incorporation of CNFp with PMMA improved the properties of the composite films, including transparency (compared with PMMA/CNF composite film), better mechanical properties, and lower wettability. Therefore, these newly developed PMMA composite films with PA-modified CNFs can serve as promising transparent reinforced plastic nanomaterials.

3.5 References

1 H. Liu, D. Liu, F. Yao and Q. Wu, *Bioresour. Technol.*, 2010, **101**, 5685–5692.

2 R. J. Nussbaumer, W. R. Caseri, P. Smith and T. Tervoort, *Macromol. Mater. Eng.*, 2003, **288**, 44–49.

3 L.-S. Chen, Z.-M. Huang, G.-H. Dong, C.-L. He, L. Liu, Y.-Y. Hu and Y. Li, *Polym. Compos.*, 2009, **30**, 239–247.

4 E. Tang, G. Cheng and X. Ma, *Powder Technol.*, 2006, **161**, 209–214.

5 A. Shalwan and B. F. Yousif, *Mater. Des.*, 2013, **48**, 14–24.

6 E. Erbas Kiziltas, A. Kiziltas, S. C. Bollin and D. J. Gardner, *Carbohydr. Polym.*, 2015, **127**, 381–389.

7 V. P. Anju and S. K. Narayanankutty, *Polymer (Guildf).*, 2017, **119**, 224–237.

8 L. Huang, Q. Wu, Q. Wang and M. Wolcott, *ACS Sustain. Chem. Eng.*, 2019, **7**, 15920–15927.

9 V. G. Gorade, A. Kotwal, B. U. Chaudhary and R. D. Kale, *J. Polym. Res.*, 2019, **26**, 1–12.

10 K. Miyagi and Y. Teramoto, *Polymer (Guildf).*, 2019, **174**, 150–158.

11 N. Jamaluddin, T. Kanno, T. A. Asoh and H. Uyama, *Mater. Today Commun.*, 2019, **21**, 100587.

12 H. Varela-Rizo, S. Bittolo-Bon, I. Rodriguez-Pastor, L. Valentini and I. Martin-Gullon, *Compos. Part A Appl. Sci. Manuf.*, 2012, **43**, 711–721.

Concluding Remarks

In this doctoral thesis, the properties of PLA and PMMA composite films were enhanced by additional of m-CNFs as fillers. These plastic composite films were developed to widen their applications in daily use. Cellulose was modified by stone grinding to produce smaller size particles (micro- to nano-size) and acylated by acid anhydrides to form hydrophobic species. Resulted from these modifications, the compatibility of m-CNFs and hydrophobic polymers (PLA and PMMA) was proven to be improved.

In chapter 1, MCC was physically modified to form CNF. It was proven that an increased grinding cycle would reduce the fiber size proportionally. The products of CNF were then acetylated by AA to form CNFa and used as filler in PLA composite films. CNFa demonstrated promising effects on PLA composite films with enhanced properties such as better transparency and higher mechanical strength compared with unmodified CNF. CNF with a diameter of 69 ± 21 nm was prepared after 5 grind cycles and characterized. Then, CNF was acetylated into CNFa by the AA with DS values from 0.62 to 1.15 based on the reaction time and amount of AA used. The optimum reaction conditions in this research are 4 hours reaction time and 75 g of AA, which produced CNFa with DS = 1.07. The compatibility of PLA films with cellulose fillers was enhanced and proved by SEM images on PLA/CNFa composite films as no obvious agglomeration was observed. CNFa (1 wt%) fillers improved the tensile strength of the films by 25% up to 37.6 ± 3.8 MPa, while neat PLA exhibited 30.1 ± 3.0 MPa. Furthermore, contact angles of PLA composite films were improved by 22.4% when CNFa (2 wt%) was added to the matrix indicated that the hydrophobicity of PLA/CNFa composite films enhanced after the addition of filler. PLA composites with CNFa with DS of 1.07 possessed several advantages based on its preparation

methods such as the efficient amount of product, higher compatibility, and better mechanical properties.

In chapter 2, the influences of three types of acid anhydrides were compared on CNF modification. Higher steric effect and lower surface area led BA to have a lower rate of reaction with CNF. Therefore, CNFa and CNFp had higher DS at the same period compared to CNFb. Acylation rates of CNFa and CNFp were almost similar with CNFp showed slightly higher DS at all studied time. Also, products of these modifications were further compared on the effectiveness as filler in PLA composite films. Higher DS of m-CNFs produced the composite films with enhanced transparencies and mechanical properties. Meanwhile, the wettability of PLA composite films was controlled by the length of the alkyl-chain substituent of m-CNFs. CNF was successfully modified into CNFp by substituting the hydroxyl group of CNF for a propionyl group from PA. By increasing the reaction time to 4 h, the DS of CNFp was improved to a value of 1.55 (51.8% acylation). PMMA composite films with CNF, CNFp, and CNFa as fillers were successfully fabricated by the solution casting technique. Comparison of transparency between composites with fillers showed that CNFp and CNFa have better compatibility with the PMMA matrix. The results obtained from images, UV-vis transmittance, and haze values confirmed that the PMMA matrix transparency was maintained. In comparison with neat PMMA and PMMA/CNF composite films, the mechanical properties of PMMA/CNFa and PMMA/CNFp were enhanced. Uniform dispersion of the CNFp and CNFa in the PMMA matrix is a key factor for this enhancement. Furthermore, the wettability of the PMMA composite films was reduced by the introduction of CNFp, resulting in a higher WCA for the PMMA/CNFp composite films. In general, the influence of CNFp and CNFa as fillers on the PMMA matrix was not very different and the transparency of the PMMA/CNFp composite films was slightly lower. Meanwhile, its mechanical and wettability properties were slightly enhanced compared to those of the PMMA/CNFa composite film. In

conclusion, the incorporation of CNFp with PMMA improved the properties of the composite films, including transparency (compared with PMMA/CNF composite film), better mechanical properties, and lower wettability.

In chapter 3, the effects of m-CNFs as fillers in PMMA composite films were studied. The influence of CNFp and CNFa as fillers for the PMMA matrix was almost similar and comparable. Furthermore, the mechanical and wettability properties of PMMA/CNFp composite films were slightly enhanced compared to those of the PMMA/CNFa composite film. Compared with unmodified CNF, the incorporation of CNFp improved the properties of PMMA composite films, including transparency, better mechanical properties, and lower wettability. Therefore, the acylation of CNF to produce CNFp will increase its compatibility with the PMMA matrix. CNF was acylated using fatty acid anhydrides with short alkyl chain substituents (C1 to C3), followed by the fabrication of PLA composite films. It was proven that CNFp has the highest rate of acylation among other m-CNFs, which 4 hours reaction time produced 31.4% CNFp, the highest among all studied parameters. PLA composite film had its transparency, mechanical, and wettability properties reduced after the introduction of CNF as filler. On the other hand, the compatibility of m-CNFs with the PLA matrix was mostly improved as proven by the characterizations mentioned in the results and discussion part. After the comparison between each film, the effects of different fatty acid anhydrides modified CNF on PLA composite films were investigated. It was demonstrated that PLA/CNFp4 composite films showed the best transparency and mechanical properties, which was mainly due to their highest DS of fillers among the films. Therefore, the DS of the fillers is the key factor to improve the properties of PLA composite films. Meanwhile, low DS of CNFb2 (0.47) displayed inhomogeneity of the matrix-filler interaction as the unmodified CNF part in CNFb2 had a more significant effect on the composite. Thus, the transparency and mechanical properties of PLA/CNFb2 composite film are considerably low when

compared with other PLA matrices with m-CNFs fillers. However, the wettability of the PLA/CNFb2 composite film was improved by the increment of the WCA reading.

In conclusion, cellulose was successfully fibrillated by a stone grinder and further esterified by using three types of acid anhydrides. Each acid anhydride possessed a different length of alkyl chain substitutions. The acylation rate of m-CNFs also varies and corresponds to their anhydrides. The main objective of these acylations was achieved by the compatibility improvement between CNF and hydrophobic polymers. Based on the analysis and characterizations, m-CNFs with good DS show better compatibility with PLA and PMMA compared to unmodified CNF.

Lists of Publications

1. **Naharullah Jamaluddin**, Yu-I Hsu, Taka-Aki Asoh, Hiroshi Uyama.

   Optically transparent and toughened Poly(methyl methacrylate) Composite Films with Acylated Cellulose Nanofiber. *ACS Omega*. **2021**, 6, 16, 10752-10758.

   DOI: 10.1021/acsomega.1c00325.

2. **Naharullah Jamaluddin**, Yu-I Hsu, Taka-Aki Asoh, Hiroshi Uyama.

   Effects of Acid-Anhydrides-Modified Cellulose Nanofiber on Poly(lactic acid) Composite Films. *Nanomaterials*. **2021**, 11(3), 753.

   DOI: 10.3390/nano11030753

3. **Naharullah Jamaluddin**, Tomonari Kanno, Taka-Aki Asoh, Hiroshi Uyama.

   Surface Modification of Cellulose Nanofiber using Acetic Anhydride for Poly(lactic acid) Reinforcement. *Materials Today Communications*. **2019**, 21, 100587.

   DOI: 10.1016/j.mtcomm.2019.100587.

Acknowledgments

I want to give the highest appreciation to my supervisor, Prof. Dr. Hiroshi Uyama for everything. His kind help and encouragement will be the most important support during my study. Moreover, I thank him for the knowledge and experience that he gave me for the past 5 years as his master and doctoral student.

Besides that, I want to thank Associate Prof. Taka-Aki Asoh and Assistant Prof. Yu-I Hsu for their guidance and advice. Other than that, they gave me the high motivation to keep my focus on track until I finished my study. Also, I deeply appreciate Prof. Dr. Hidehiro Sakurai and Prof. Dr. Akinori Saeki for their care and valuable review of this doctoral thesis. Their advice and comments have been evaluated and utilized for the improvement of this dissertation.

Next, I am grateful to Ms. Yoko Uenishi and Ms. Tomoko Shimizu for their assistant as secretaries of Uyama Laboratory. I am thankful for the previous and current Uyama Laboratory members (including visitors), acquaintances in the Applied Chemistry department, and friends in Osaka University. Then, I like to thank the Japanese government through the Ministry of Education, Culture, Sports, Science and Technology of Japan (MEXT Japan) for the scholarship given.

The most special tribute is given to my supporting wife, Nur Aqeela Salfarina, along with our precious son, Aufa Nufail, who always kept me motivated during our time in Japan. Furthermore, I would like to thank Jamaludin & Latifah (parents), Ab Razak & Tianinun (parents-in-law), my siblings, in-laws, nieces, and nephews. Their good support and motivation are the main factors for me to keep moving forward and complete my doctoral study here, at Osaka University. I love you with all my heart. Alhamdulillah.

June 2021

Naharullah Bin Jamaluddin